SANDIA REPORT
SAND2005-0874
Unlimited Release
Printed February 2005

LDRD Final Report on Continuous Wave Intersubband Terahertz Sources

M.C. Wanke, R.J. Foltynowicz, E.W. Young, M.A. Mangan, C.T. Fuller, S. Samora, J.L. Reno, L. Stephenson, J.J. Hudgens

Prepared by Michael C. Wanke
Sandia National Laboratories
Albuquerque, New Mexico 87185 and Livermore, California 94550

Sandia is a multiprogram laboratory operated by Sandia Corporation,
a Lockheed Martin Company, for the United States Department of Energy's
National Nuclear Security Administration under Contract DE-AC04-94AL85000.

Approved for public release; further dissemination unlimited.

Issued by Sandia National Laboratories, operated for the United States Department of Energy by Sandia Corporation.

NOTICE: This report was prepared as an account of work sponsored by an agency of the United States Government. Neither the United States Government, nor any agency thereof, nor any of their employees, nor any of their contractors, subcontractors, or their employees, make any warranty, express or implied, or assume any legal liability or responsibility for the accuracy, completeness, or usefulness of any information, apparatus, product, or process disclosed, or represent that its use would not infringe privately owned rights. Reference herein to any specific commercial product, process, or service by trade name, trademark, manufacturer, or otherwise, does not necessarily constitute or imply its endorsement, recommendation, or favoring by the United States Government, any agency thereof, or any of their contractors or subcontractors. The views and opinions expressed herein do not necessarily state or reflect those of the United States Government, any agency thereof, or any of their contractors.

Printed in the United States of America. This report has been reproduced directly from the best available copy.

Available to DOE and DOE contractors from
U.S. Department of Energy
Office of Scientific and Technical Information
P.O. Box 62
Oak Ridge, TN 37831

Telephone: (865)576-8401
Facsimile: (865)576-5728
E-Mail: reports@adonis.osti.gov
Online ordering: http://www.osti.gov/bridge

Available to the public from
U.S. Department of Commerce
National Technical Information Service
5285 Port Royal Rd
Springfield, VA 22161

Telephone: (800)553-6847
Facsimile: (703)605-6900
E-Mail: orders@ntis.fedworld.gov
Online order: http://www.ntis.gov/help/ordermethods.asp?loc=7-4-0#online

SAND2005-0874
Unlimited Release
Printed February 2005

LDRD Final Report on Continuous Wave Intersubband Terahertz Sources

Michael C. Wanke, Erik W. Young, Michael A. Mangan, Charles T. Fuller,
Sally Samora, and James J. Hudgens
Photonic MicrosystemsTechnologies Department

R.J. Foltynowicz
Lasers, Optics and Remote Sensing Department

John L. Reno, Larry Stephenson
Semiconductor Material & Device Sciences Department

Sandia National Laboratories
P. O. Box 5800
Albuquerque, NM 87185-0603

Abstract

There is a general lack of compact electromagnetic radiation sources between 1 and 10 terahertz (THz). This a challenging spectral region lying between optical devices at high frequencies and electronic devices at low frequencies. While technologically very underdeveloped the THz region has the promise to be of significant technological importance, yet demonstrating its relevance has proven difficult due to the immaturity of the area. While the last decade has seen much experimental work in ultra-short pulsed terahertz sources, many applications will require continuous wave (cw) sources, which are just beginning to demonstrate adequate performance for application use.

In this project, we proposed examination of two potential THz sources based on intersubband semiconductor transitions, which were as yet unproven. In particular we wished to explore quantum cascade lasers based sources and electronic based harmonic generators. Shortly after the beginning of the project, we shifted our emphasis to the quantum cascade lasers due to two events; the publication of the first THz quantum cascade laser by another group thereby proving feasibility, and the temporary shut down of the UC Santa Barbara free-electron lasers which were to be used as the pump source for the harmonic generation.

The development efforts focused on two separate cascade laser thrusts. The ultimate goal of the first thrust was for a quantum cascade laser to simultaneously emit two mid-infrared frequencies

differing by a few THz and to use these to pump a non-linear optical material to generate THz radiation via parametric interactions in a specifically engineered intersubband transition. While the final goal was not realized by the end of the project, many of the completed steps leading to the goal will be described in the report.

The second thrust was to develop direct THz QC lasers operating at terahertz frequencies. This is simpler than a mixing approach, and has now been demonstrated by a few groups with wavelengths spanning 65-150 microns. We developed and refined the MBE growth for THz for both internally and externally designed QC lasers. Processing related issues continued to plague many of our demonstration efforts and will also be addressed in this report.

Table of Contents

LDRD final report on continuous wave intersubband THz sources 3
Abstract 3
Table of Contents 5
Background and Motivation 6
Accomplishments 8
Device Modeling Tool Development 8
MBE Growth Development 9
Device Fabrication Development 11
Device Mounting 13
MIR and THz Measurement Capability Development 14
Non-linear Optical Properties Charactization Set-up 15
MIR Lasers 17
THz Lasers 19
Publications 21
Invited Presentations 22
Appendix II: Wet Etches 23
Appendix III: Insulator Tests 34
Insulator tests versus anneal temperature: 34
Insulator tests versus material 36
Summary 40
Distribution 41

Background and Motivation

The moniker "terahertz" refers to frequencies of 10^{12}, or one trillion, cycles per second. The 0.1 – 10 terahertz (THz) region of the electromagnetic spectrum is relatively little-explored, for the following reason: *the terahertz regime lies in the frequency gap between conventional electronic devices, at the low frequency side, and conventional optoelectronic devices, at the high frequency side.* Electronic devices, dependent on electron spatial transport across base thicknesses or gate lengths, can reach up to ~100 GHz (0.1 THz). Optoelectronic devices, on the other hand, are typically based on electronic energy transitions across a semiconductor band gap, and can get down to frequencies of 25 THz without too much difficulty. Between these two lies the THz regime, where conventional compact semiconductor device approaches fail. Existing approaches are either very large, heavy, and expensive (molecular gas lasers), highly inefficient (sources based on mixing), very slow (detectors), or are otherwise seriously deficient.

We intend to develop *a comprehensive terahertz (THz) technology infrastructure* relevant to national security needs. Our goal is to establish the world's leading technology hardware/systems base for exploiting unique capabilities of THz radiation for multiple national security applications. Potential applications include high selectivity molecular vapor identification for non-proliferation assessment, explosives detection, and chem./bio threat detection; high bandwidth covert terrestrial and space-based communications; airport portal screening for concealed objects; through-wall imaging and inspection of neutron tubes; detection of incipient voltage breakdown in firing sets; and burgeoning other civilian applications.

Sources of coherent THz frequency (*i.e.* 0.1 to 10 THz) electromagnetic radiation with requisite power levels, frequency agility, compactness and reliability represent the single greatest obstacle in establishing a THz technology base. To be truly useful, a coherent THz source should be as compact, reliable, and frequency versatile as familiar solid-state rf/microwave and infrared/visible source technologies, and be able to deliver average power at least in the 10 to 100 mW range. Current generally available THz source technologies are often extrapolations of either microwave electronic oscillators (*e.g.* Gunn diodes, multipliers, backward wave oscillators) or optically-based infrared lasers (*e.g.* free electron lasers, molecular gas lasers). These can usually deliver only some of the features called for in conceivable THz applications, and thus severe and highly constraining compromises inevitably have to be made. Since the beginning of this project semiconductor-based quantum cascade lasers (QCL's) have evolved from only a promising candidate for a potential THz source to becoming the best semiconductor THz source available between 2 and 5 THz.

At the beginning we planned on pursuing two thrusts toward THz sources. In one of our approaches, we planned to mix two quantum cascade lasers operating in the far-infrared using resonantly designed intersubband transitions. The other approach was to examine non-linear transport in superlattices to up-convert microwave power by efficient harmonic generation enhanced by an intersubband transition. Both approaches were based on driving *intersubband* transitions. Traditionally, optical devices have relied on *interband* transitions, i.e. transitions between the valence and conduction bands. At THZ energies, corresponding to 3-30 meV, devices based on interband transitions do not exist due to a variety of difficulties. Rather, one

must rely on the new approach of intersubband transitions, i.e. transitions between quantized energy levels defined in quantum wells in the conduction band. This approach, commonly referred to as “bandgap engineering”, is thought by many to represent the future of semiconductor electronics. Already, this approach has yielded tremendous advances in detectors, resulting in the invention and development of the quantum well infrared photodetector (QWIP), which has resulted in improved detectivities, planar arrays, and wavelengths as long as 28 microns. Another successful example of intersubband technology is the quantum cascade laser (QCL), which is revolutionizing the field of mid to far-infrared lasers.

Quantum cascade lasers are a type of semiconductor laser. The typical size is on the order of a couple of millimeters long. In contrast to typical semiconductor lasers which operate as bi-polar devices, QCLs are generally unipolar devices in which lasing occurs via electronic transitions between states all within the conduction band (*i.e.* intraband transitions). Since the frequency of the generated light is dependent on layering geometry, a very wide range of frequencies can be accessed within the same material system allowing devices to be fabricated using mature III-V semiconductor alloy systems. Output powers have approached 10 W for a single laser near 10 micron operation and maximum cw operating temperatures can now exceed room temperature. Currently wavelength coverage has been demonstrated between 3.5 – 24 microns and 65 -160 microns. Due to the nature of the light generation mechanism, QC lasers can exhibit very narrow linewidths which is beneficial for spectroscopy and in our case beneficial for non-linear pumping.

Figure **Figure 1** shows the bandstructure for two periods for a superlattice type QC laser. The basic principle can be explained as follows: Electrons are injected from the upper right into a high lying quantum state. The electron drops to a lower state by emitting a photon. After this the electron is transported to the upper state in the next period where the process begins again. *The photon energy is dependent on the widths of the wells and barriers, which can be tailored by the design*. Due to the nature of the transport, we can stack as many periods as desired on to of each other; if all the active regions are the same this increases the power, or alternatively we can stack regions with different transition energies and obtain multiple frequency lasing from the same waveguide.

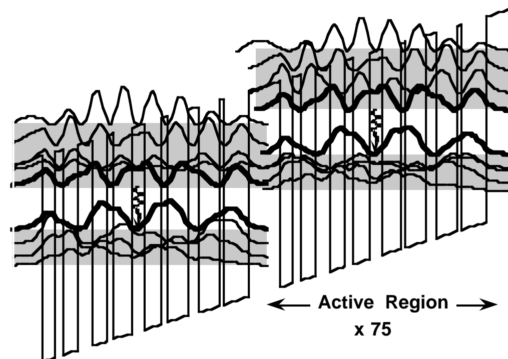

Figure 1 - Bandstructure of a QC laser operating at 11µm (Wanke et.al. APL). The dark lines represent the states involved in the optical transition.

Just after the program began, a former colleague of the author demonstrated the first THz quantum casade laser[1]. After that our focus shifted away from harmonic generation and onto two separate approaches based on QC lasers. The first was still the non-linear difference frequency

[1] R. Kohler, et.al., *Nature*, **417**, 156 (2002)

mixing of two mid-IR lasers, and the second was to continue earlier work pursuing direct THz emission from a QC laser.

In the first thurst, a quantum cascade (QC) laser simultaneously emits two mid-infrared frequencies differing by a few THz. These are used to pump a non-linear optical material to generate THz radiation via parametric interactions. As a specific example we wanted to explore difference-frequency-generation by three-wave mixing in a specifically engineered intersubband transition. In Fig. Figure 2 we show schematically an intersubband transition designed to enhance the mixing. The figure shows three quantum states and their relation to the input photon energies $\hbar\omega_1$, $\hbar\omega_2$, and the THz photon energy ($\hbar\omega_1$-$\hbar\omega_2$). Similar designs have demonstrated more than 4 orders of magnitude improvement in conversion efficiency compared with a bulk crystal made of the same material. Although we wish to focus on intersubband transitions for the frequency conversion, other materials exhibiting large nonlinear mixing coefficients will also be explored. Non-resonant materials may provide more tunability than a resonant design. This will also allow us to utilize the demonstrated tuning capabilities of single mode QC lasers, which can be tuned by more than one THz.

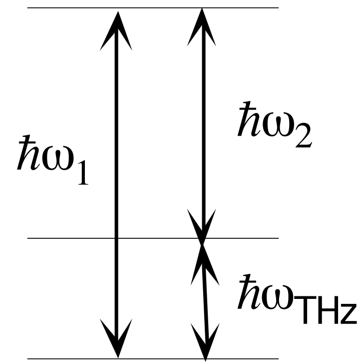

Figure 2 – Intersubband transitions designed to resonantly enhance THz generation by DFM

In general, the efficiency of the frequency mixing increases with the pump power, thus we will examine approaches to integrate the mixing material such that it shares the same waveguide as the quantum cascade laser, where the intracavity field strength is the strongest. To begin this work we first needed to develop MIR QC lasers.

Our second approach is to pursue QC lasers that operate at terahertz frequencies. This is simpler than a mixing approach, and has been demonstrated with operation wavelengths spanning 65-150 microns. However, they are more difficult to design and have reliability and reproducibility issues. Currently these lasers only operate below 140 K and although already operating above expected temperatures further increases are not immediately likely. Power levels, however, have already reached 30 mW, and will probably always exceed power output from mixed sources. Thus the two approaches may have complementary application interests.

Accomplishments

Device Modeling Tool Development

Quantum-cascade lasers are designed using a self-consistent Schroedinger-Poisson solver. The basic program necessary to make these calculations existed at the outset of the program, but was limited in capability. The code was translated completely into the C programming language

while removing many of the previous machine and programmed limits that prevented exploration of large structures.

While the performance of quantum cascade lasers depends heavily on the design concept of the region (the active region) in the semiconductor where the lasing takes place, much of the actual laser design not in this region (the injector region) is fairly standardized for the mid-IR. One of these standards was added to the program so that the computer could generate these regions automatically, saving a fair amount of time in designing and adding a layer of consistency not present before.

A few other changes to the program were made to speed the execution time of the run, and extra output files and macro scripts were generated to speed the analysis of the designs created. The enhancements to the program also aid in the design and analysis of the superlattices required for the harmonic generation measurements.

Beyond cosmetic changes, other physical parameters were updated and added[2] to increase the accuracy of the designs, to enable designs with alternative material systems, and to add capabilities to account for changes from material strains using Model Solid Theory. Extra routines were added to allow construction of very think strain balanced layers using methods outlined by Van de Walle[3] and Ekins-Daukes.[4]

Analysis routines were added to provide quantitative comparisons between laser designs. This help to ensure consistency between lasers operating at different wavelengths that is required for the ultimate goal of running two lasers with different wavelengths in the same waveguide core. Before this addition comparison of designs was strictly qualitative and many designs though to be similar could have vastly different performance.

MBE Growth Development

In collaboration with Professor Qing Hu's group at MIT, we have developed techniques to consistently and reproducibly grow THz quantum cascade lasers (QCLs) by MBE. These structures are quite complicated and quite thick. They are comprised of 2500 or more individual layers with thickness as small as 3 monolayers and a total thickness of more than 10μm. The growth times range from 16 to 20 hours for a complete structure. Given this growth challenge, three areas have shown themselves to be of great importance: interface quality, accuracy and uniformity. Each will be addressed individually.

This is a vertical transport device so carriers must pass through the large number of interfaces in the structure (>2500). To avoid carrier scattering, the interfaces must be as smooth as possible. In addition there is a high Al content layer at the bottom of the structure that serves as an etch-stop layer. Due to the high Al content this layer tends to be rough and all the other layers are grown on top of it. This roughness can be removed and the growth surface smoothed during the

---

[2] I. Vurgaftman, et. al., *J. Appl. Phys.,* **89**(11), 5815 (2001)
[3] C.G. Van De Walle,, *Phys. Rev. B*., **39**(3), 1871 (1989)
[4] Ekins-Daukes, et.al., *Crystal Growth and Design*, **2**(4), 287 (2002)

growth of the GaAs contact layer that immediately follows it. That thick contact layer is grown with periodic growth interrupts that give the surface time to anneal and smooth. During the highly layered active region the growth conditions must be adjusted so as to provide the optimal interface quality and smoothness. These interfaces are similar in type, but not number, to the interfaces that are found in the high mobility structures that have previously been developed at Sandia. The same growth temperature and Group V to III ratio are used from that work. These techniques produce smooth high quality interfaces throughout the structure.

For QCLs to operate as designed, the subbands must align precisely. This means that all parameters that affect the position of the subbands must be grown with great accuracy. The three parameters that most affect the subband positions are the individual layer thicknesses, the Al concentration in the barriers and the doping level in the active region. Calibration procedures have been developed for each of these. The standard technique used by the MBE community to calibrate growth rates is the use of RHEED intensity oscillations. This technique is easily used and reproducible for any given cell but it is not highly accurate. Geometry factors also influence the measurement so that the actual growth rate differs from that measured by RHEED by varying amounts for different cell positions. X-ray diffraction has been used to determine a correction factor between the actual growth rate and that measured by RHEED. This growth rate correction factor ranges from -7% to +2% depending on the cells used and also on the RHEED sample. RHEED is then used on a daily basis to assure reproducibility. This allows our layer thicknesses to be within ±1% of that specified by the device design. The Al concentration in the AlGaAs alloy barriers is also usually determined by using RHEED measured growth rates. The ratio of the Al growth rate to the total growth rate of Ga plus Al is the value of the Al concentration that is used commonly within the MBE community. A test structure that can be used with low temperature photoluminescence to accurately determine the actual Al concentration has been developed. This allows the determination of a correction factor for the Al mole fraction. This correction factor has been found to vary from -0.008 to +0.012 depending on the cells used and also on the RHEED sample. RHEED is then used on a daily basis to assure reproducibility. This allows our Al mole fraction to be within ±0.001 of that specified by the device design. The doping levels in the active region of THz QCLs are typically 1-4 x $10^{16}/cm^3$. Published work in mid-infrared QCLs indicates that variations in the doping level of ±10% influence the performance characteristics of the laser. Normal accuracy for doping in MBE structures is ±100%. Precalibration structures grown using the same growth conditions as in the QCLs allow the doping level to be set within ±10% of that specified.

For QCLs to operate as designed, not only do the subbands need to align precisely but the alignments must be the same throughout the active volume of the device. This means that the sample must be grown with a high level of uniformity in both the horizontal and the vertical (growth) directions. There are two types of horizontal uniformity that influence QCLs, thick layer and thin layer. The factor influencing the thick layer horizontal uniformity is the design of the MBE system and can not be easily changed. The thick layer horizontal uniformity for the system used in this project is ±0.35% over a 3” wafer. The thin layer horizontal uniformity has not been measured but the factors affecting have been determined. It is influenced by both the rotation rate and the opening and closing speeds of the Al cell shutter. Both these have had to be increased significantly higher than is standard to achieve operating QCLs. The vertical uniformity is affected by changes in the growth rates due to cell depletion. Using measurement

before and after growths, the growth rate change due to cell depletion rate was measured to be 0.6% per micron of growth. This rate is too large for successful THz QCLs but is too small to be corrected for using standard temperature controllers. The temperature controllers were modified to allow a temperature ramp rate of 0.1°/hr. This allows the growth rate to be kept within ±1% for the entire 10 to 11 m structure.

Using the calibration procedures, correction factors, growth conditions and equipment modifications determined in this project, THz QCLs have been grown consistently and reproducibly.

Device Fabrication Development

Conceptually the processing requirements for QC lasers is relatively straightforward. In practice, however, many difficulties arose, some expected and some not, requiring significant development efforts. Robust solutions for all the steps are still lacking and have limited the progress in other areas of the project due to lack of sample throughput.

The biggest stumbling block and one that still appears intermittently is etching the laser waveguides. Other areas of difficulty included metal delamination, insulator failure, and ohmic contact annealing.

The two types of lasers (direct THz lasers, and MIR lasers for pumping a THz mixer) have different etching difficulties. The key to successful THz lasing is reduction of waveguide losses. Two solutions for low-loss waveguides have been demonstrated successfully to date: a thin highly doped GaAs layer between the laser core and an insulating substrate or sandwiching the laser core between two metal contacts after removing the substrate completely.

We pursued the first approach requiring growth of a relatively thin layer (0.5 microns) of highly doped GaAs between the laser and an insulating GaAs substrate. This layer serves as a confinement layer for the optical mode and as the electrical contact to the bottom of the laser. The rest of the THz laser structure can range in thickness from 10 to 20 microns. Thus in order to make contact with the highly doped bottom layer, the etch must be able to decend 10 to 20 microns and stop within +/-100 nm of the top of the high doped layer. Much deeper and the contact is broken and much shallower the contact becomes highly resistive at best. While the RIBE tool has this capability deep

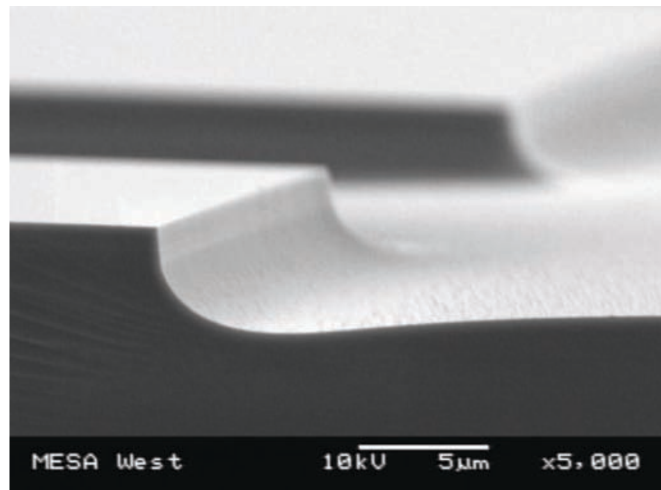

Figure 3 - EB 2013 demostrates the undesirable trenching. This laser in InP based but similar effects are observed in GaAs devices.

etches like this significantly lower the lifetime of the acceleration grids, and had too much impact on other users. The Semigroup RIE tool demonstrated too much non-uniformity of etch depth across the wafer and was also difficult to get reliable end-point detection readings. The ICP etcher should be capable of this etch, but until the very end of the project was not available for use and still does not have the required end-point detection capability required. Thus development effort was focused on wet etches. THz lasers do not require smooth sidewalls or a particular sidewall shape so the main issue with etching these lasers is trenching, the tendency to overetch at the base of the etched mesa (see Fig. Figure 3) A few of the many etches tried are displayed in appendix 2.

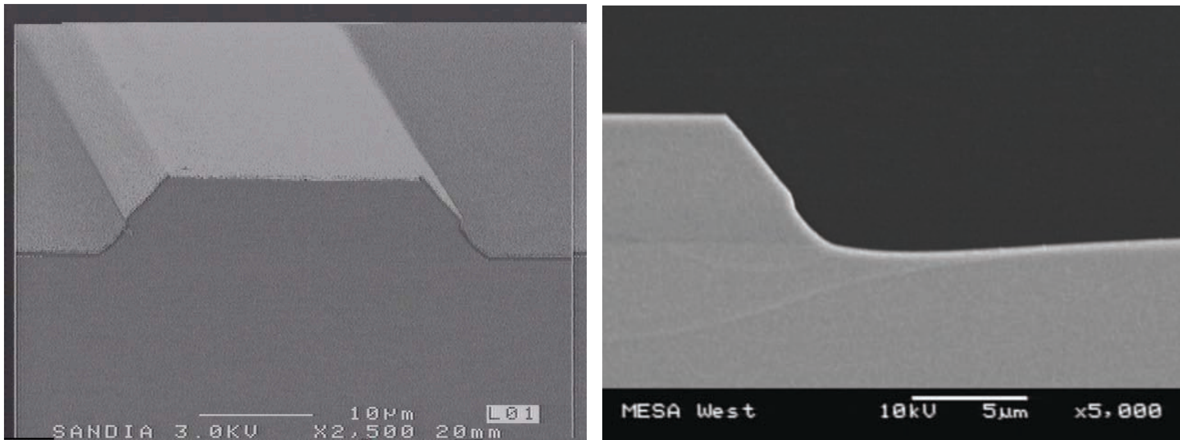

Figure 4 - EA 0991 (left) showing the kink in the sidewall. Close examination show the kink is undercutting and metal does not cross the kink continuously. EA 0993 on the right shows the kink and some trenching near the mesa bottom as well.

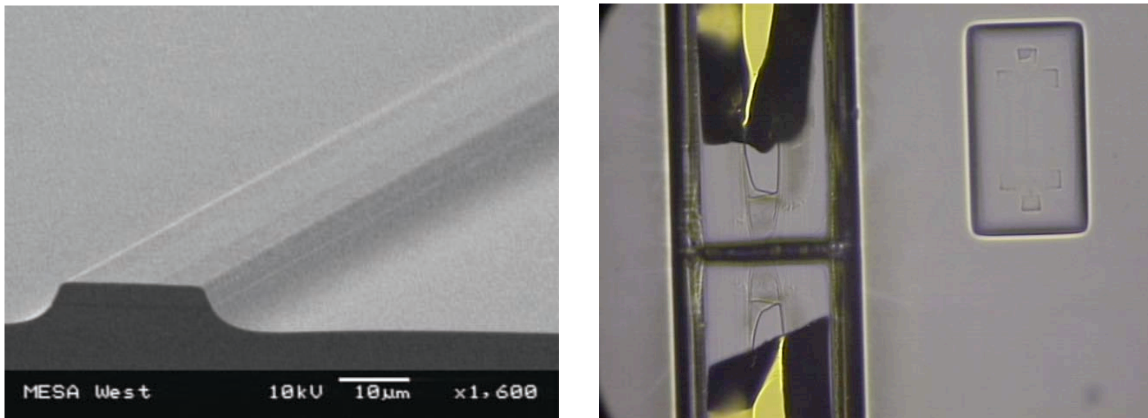

Figure 5 - Same etch chemistry with very different results where the metal presence is the only significant difference between them. (EA 0980 and EA 0873 respectively)

The MIR QC lasers had different difficulties. Here the substrate is conducting so the etch depth is no longer a critical parameter. The laser stripe widths however, are on the order of 10-20 microns wide which is too small to bond wires to directly. Thus a contact pad is placed off to the side of the laser which must be connected electrically to the top of the laser stripe. For this to happen the sidewalls of the laser need to have no overhangs. In addition the wavelength of light in the laser is only a couple microns, so surface features on the walls can influence the

performance of the laser. Thus smooth sidewalls are also desirable. Many of the etches tried for this would undercut mesa with resulting breaks in the metal from the contact pad to the mesa top. Figure Figure 4 shows a subtle undercut.

Many etches would work on test pieces of real samples when no metal was present on the samples, but then on the real devices with metal present the etch behavior would sometimes be radically different (see Fig. Figure 5).

Metal delamination was a separate cause for device failure. This turned out to be a combination of two effects. After close examination the first turned out actually to be a a failure of the insulator adhesion to the sample and will be discussed below. The second was never completely resolved, but was resolved by switching evaporators from EG2 to the new Temescal. This leads me to believe that either the sources in the EG2 were contaminated or the system is just a lot dirtier in general. A post-op on a couple samples of supposedly Ti-Au evaporation turned up a significant amount of molybdenum, apparently confirming the contamination scenario.

Insulator failure is mostly fixed at this point, but still occasionally occurs. This general failure is the creation of bubbles in the insulator when the metal contacts are annealed to make ohmic contact. Examples of this failure are described in appendix 3. The outcome of these bubbles ranges from the contact metal peeling off preventing contacts from being bonded to the device, to allowing conductive shorts through the insulator shunting the current around the laser core. Going to lower temperature anneals whenever possible minimizes the bubbling in SiN films, but to get reliable films on SiO2 required deposition of the films at an elevated temperature of 350C.

Device Mounting

QC lasers generate a lot of waste heat and their performance degrades as their temperature rises. This is especially important in THz QC lasers where the maximum operating temperature is 140 K. Thus heat sinking must be considered even for test samples being tested at cryogenic temperatures.

As a minimum effort, we mount our lasers directly onto gold-plated copper blocks using indium solder to between the laser substrate and the block. The bottom of the laser substrates have metal evaporated onto them to provide a metal surface for the solder to adhere to. In the case of MIR lasers, this metal layer also serves as a contact for the laser.

The mounting proceeds as follows. First the processed chip containing multiple lasers are scribed and separated into smaller pieces using a Loomis scribe and break machine. Each piece contains on the order of 6 lasers of the desired length. The cleaved facets of the chip act as the mirrors for the laser stripes and care must be taken not to scratch them or get solder on them in the following steps.

Every laser bar is visually inspected for surface damage and cleave quality. After the bar passes inspection a gold plated copper mount is prepared. First the center of the mount is found and scribed with a sharp tool. The mount is then cleaned with isopropyl alcohol and mounted on a

chuck. The chuck is heated to 60 degrees Celsius and a small amount of flux[5] is applied using a sharpened wooden tool. An indium foil solder perform[6] is then sized with a razor blade to typically 1 by 5 millimeters and carefully aligned on the mount center scribed edge. The solder is fixed with the vacuum pick up tip forcing intimate contact between the solder and the mount. Another small amount of flux is placed on top of the solder and this assembly is heated to seventy degrees Celsius. The vacuum tip is cleaned with isopropyl and the laser bar is picked up by the tip. Then the laser is roughly aligned to the scribe and placed on the mount. Using another machined wooden tool the laser bar is nudged into final position. The vacuum tip is now placed on the center of the laser bar and weighted with 30 grams. The temperature of the chuck is slowly increase 20-30 degrees Celsius at a time and visually monitored until the solder wets the junction and flows. The assembly is cooled then visually and mechanically inspected. After inspection gold contact pads are attached with varnish. The assembly is again mounted on the chuck and wire bonded. Up to fourteen bond wires are attached to each laser. The result of the above process as shown in fig. Figure 6 has proven to survive in repeated cryogenic temperature cycling as well.

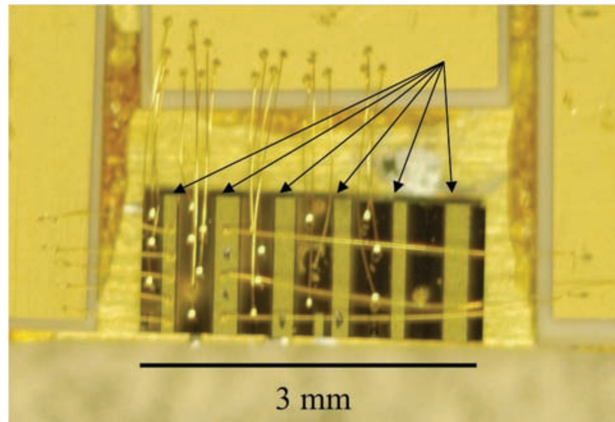

Figure 6 - Six THz lasers on a chip (the brighter gold stripes pointed at by arrows), soldered to a gold plated copper block, and wire bonded to contact pads held down with GE varnish

MIR and THz Measurement Capability Development

Since the goals of this project were to explore and develop a terahertz source, a new and emerging technology at Sandia, it also required expanding Sandia's existing measurement infrastructure. A terahertz absorption and emission spectroscopy laboratory was assembled. The center of this new capability is a FTIR (Fourier transform infrared) spectrometer with the optical path completely in vacuum. We have extended this vacuum system on one end to incorporate a selection of detectors: MIR DTGS, THz DTGS, slow and fast MCT's for MIR, slow THz Si, and fast THz Nb Bolometer. The fast detectors enable time resolved measurements with time resolution down to a ns. The fast time resolution is useful for watching the temporal dynamics of the laser output which aids in exploring self-heating effects. On the other end, we have incldueed an optical bench and cryostat for inserting the light from emission samples (lasers, LEDs, etc.). The cryostat allow sample temperature control between 4K and 400K. The cryostat mount was engineered to allow insertion into the middle of the FTIR as well, to enable absorption measurements, adding another characterization tool.

We rewired our Bruker 66v FTIR spectrometer to allow for external use of lock-in amplifiers for the instruments internal detectors. This allows us to better measure the spectra of weak signals,

---

[5] Superior Supersafe No. 30 Flux, Superior Flux and Mfg. Co., Cleveland, Ohio, (216) 461-3315
[6] Indium Preforms Alloy 3000, Coining of America, Saddle Brook NJ, (201) 791-4020

thereby allowing us to capture more information. This helps analyze new designs that do not lase but exhibit weak luminescence.

The associated electronics necessary (pulse generators, boxcar integrators, oscilloscopes, lock—in amplifiers, etc.) for these experiments were added. In order to test all the fabricated samples in a timely manner, we also improved the data acquisition software, and can now automatically take L-I-V curves (light and voltage vs. current measurements), at various temperatures, pulse widths and duty cycles. This has significantly shortened the time required for complete laser characterization. This terahertz laboratory is a key component of future work at Sandia in this spectral.

Non-linear Optical Properties Charactization Set-up

In order to develop continuous wave THz sources based on the difference frequency generation (DFG) approach, we need to characterize the optical properties of candidate non-linear media in the THz regime. We were unable to model these materials, due to the lack of available material parameters in the THz regime. To provide these material parameters we built a THz-time domain spectroscopy (THz-TDS) system. This system will allow us to accurately measure optical properties such as index of refraction that can then be used to model the DFG mixing process.

We initially pursued a THz-TDS (time domain spectroscopy) system based on photoconductive switching of LT-GaAs utilizing short laser pulses. Before building this system, we needed to characterize the optical and electrical properties of LT-GaAs so we can reliably fabricate these switches.

1) We built a time-resolved reflectivity apparatus that measures carrier lifetimes in semiconductor materials. We were successful in measuring the trapping time of the carriers from the conduction band to the mid-gap states in LT-GaAs. The carrier lifetimes were measured for LT-GaAs samples (EA0874, EA0875, EA0876, EA1006, EA1007, and EA1008) grown at 250°C and rapid thermal annealed for 1 min at temperatures of 500°C, 600°C and 700°C. The excitation wavelength for these measurements was 800 nm from a 76MHz Ti: Sapphire laser with a 116 fs pulsewidth.

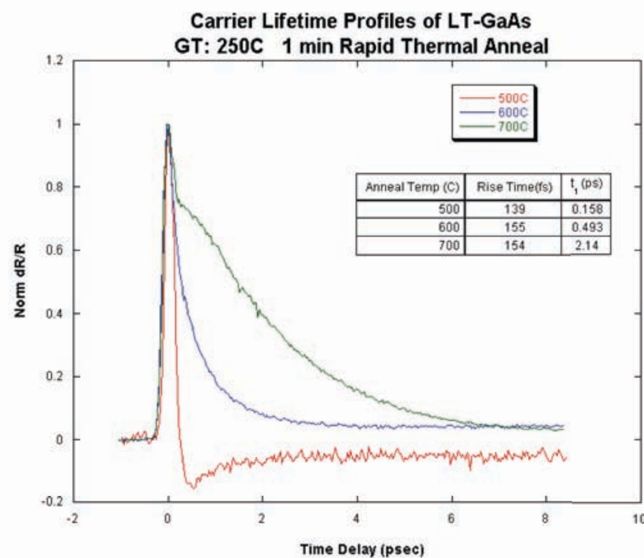

Figure 7 – Carrier Lifetime Profiles of LT-GaAs grown at 250 C and rapid thermal annealed at 500C, 600C, and 700C.

The results show that as we increase the annealing temperature, the trapping lifetime gets longer (see Fig. Figure 7) For our application, we want the growth conditions such that we have the shortest lifetimes because that will give us the greatest resolution in our THz detection. The conditions that result in the shortest lifetime was a growth temperature of 250°C and an anneal temperature of 500°C with a trapping time of 158 fs.

2) We conducted electrical testing of the LT-GaAs to determine reliable operation as a switch. The dark resistivity as a function of DC bias resulted in resistivities increasing with anneal temperatures. The best performers were LT-GaAs grown at 250C and rapid thermal annealed at 600C and 700C. However the growth conditions for LT-GaAs that gives the best performing switch depends on getting the shortest lifetime with highest resistivity. With those criteria, the sample grown at 250C and annealed at 600C is the best performer with a carrier lifetime of 493 fs and a dark resistivity of 10^8 ohm cm with a 40 V DC bias, 0.04 cm^2 area and 0.2 cm distance between contacts.

3) We completed the design work for the THz antennas required for switch operation and fabricated the switches.

Other projects arose requiring broader bandwidth that the switches provided and more time was spent converting the system to one based on electro-optical sampling instead of switches.

Currently operating at Sandia is a THz-TDS spectrometer that generates broadband, THz pulses via optical rectification in a <110> ZnTe crystal. The THz pulse propagates through a sample and is focused onto another <110> ZnTe crystal detector. The detection scheme is based on electro-optic sampling. By varying the time delay between pulse generation and detection, we monitor the change in polarization of a probe beam interacting with the ZnTe crystal whose birefringence has been modulated by a co-propagating THz pulse. The polarization change in the probe beam is proportional to the electric field strength of the THz pulse. Therefore, we measure a time domain profile of the THz electric field strength versus time delay. To obtain spectral information on the sample, a fast Fourier transform conversion is done.

The THz-TDS technique measures the time varying electric field strengths of THz pulses; therefore both spectral amplitude and phase can be unambiguously determined from FFT analysis. This information allows for the determination of complex components of optical properties such as index of refraction without the use of Kramers-Kronig relations and the associated extrapolations and uncertainties. The detection is also coherent with the incident pulse. Thus the thermal background of THz emitters becomes negligible since the detector only stays on as long as the pulse duration. In the THz-TDS method, a broad frequency spectrum is collected essentially at one time. The spectral range of the present system is about 0.3 to 3 THz.

This set-up is now being routinely used for various material characterization including obtaining THz spectral of energetic materials in the vapor phase.

MIR Lasers

As decribed earlier mid-infrared lasers are needed for the non-linear mixing approach towards THz generation. The lasers we grew and fabricated for this effort are shown in the following table. We wanted a few different frequencies for mixing purposes and enough material to develop processing recipes and waveguide designs such as DFB's that will eventually be used for generation of single mode operation.

Sample Number	Design Frequency (m)	Laser Operation?
EA 0775	9.4	Yes
EA 0980	11	No-Bad growth
EA 0982	11	Yes
EA 0993	12.6	No-Bad Growth
EA 09995	12.6	Yes
EA 0996	12.6	Yes

Besides use as pump souces for THz sources, these lasers have extensive promise for national security missions by themselves, and the development of this capability at Sandia will hopefully lead to further work in this direction.

Typical sample characterization results relevant for our needs are shown below, including spectra from Sandia's first QCL (fig. Figure 8) , light-current-voltage (LIV) curves (fig. Figure 9), frequency shifting with temperature (fig. Figure 10), and mode dependence on current(fig. Figure 11). While we did calculate the DFB (distributed feedback) structures required, including the periodicity, etch depth, and waveguide parameters, that we need for single mode operation due to the remaining processing difficulties single mode operation has not yet been demonstrated.

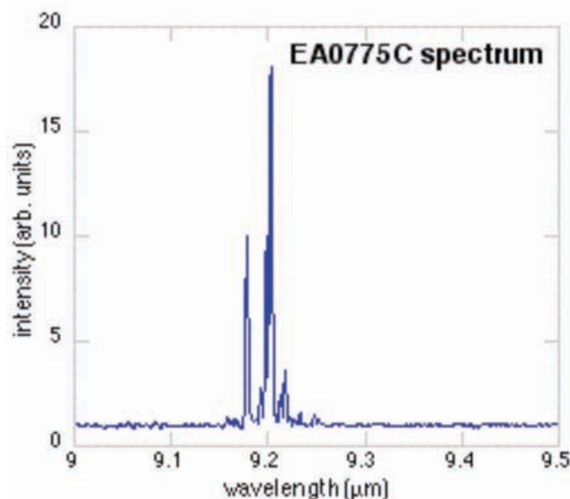

Figure 8 - Typical multimode Fabry-Perot spectrum of MIR QC laser with cleaved facets

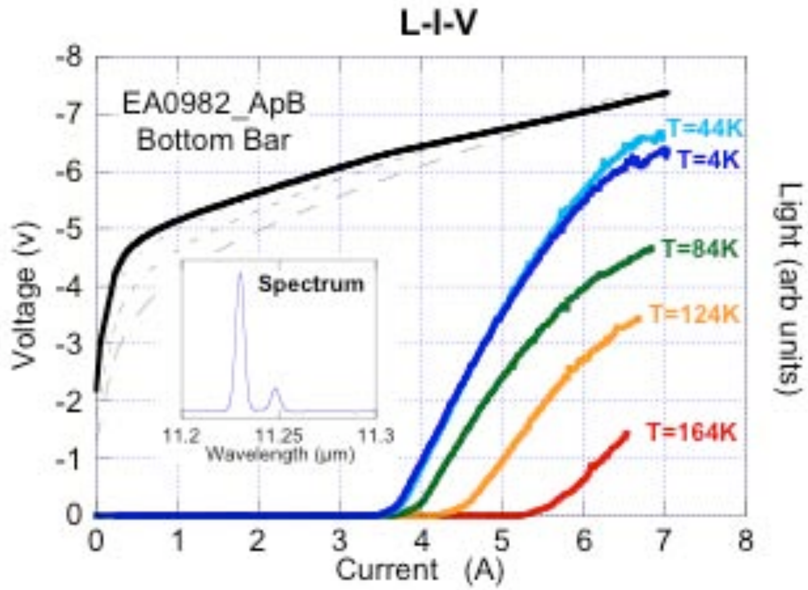

Figure 9 – L-I-V of sample EA 0982 showing temperature dependence of threshold current. The inset shows the spectrum just above threshold.

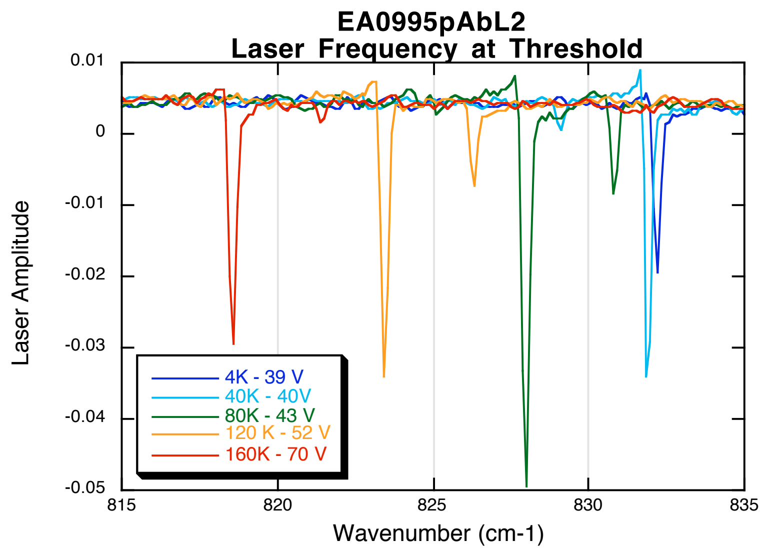

Figure 10 - Frequency dependence of laser output on temperature

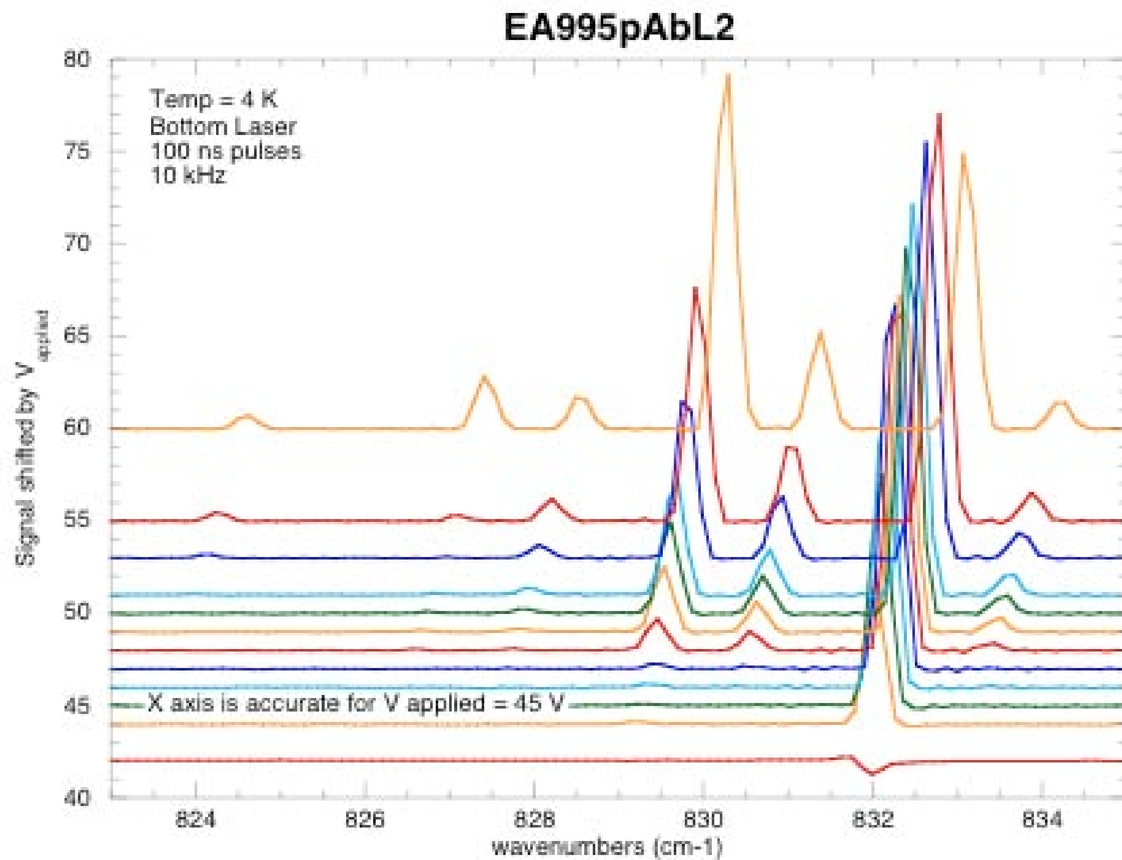

Figure 11 - Evolution of mode structure vs applied voltage

THz Lasers

As discussed in the growth section, Sandia has developed and mastered the growth capabilities necessary to grow these lasers. Figure 12, shows the structure of one of the lasers grown by Sandia (designed at MIT) Gloabally, recent results in GaAs/AlGaAs multilayered structures grown on GaAs substrates demonstrated CW devices lasing between 2.5 to 4.5 THz, with continuing effort directed at broadening this coverage further. Most impressively, CW power emission has been reported to exceed 30 mW, which is comparable to

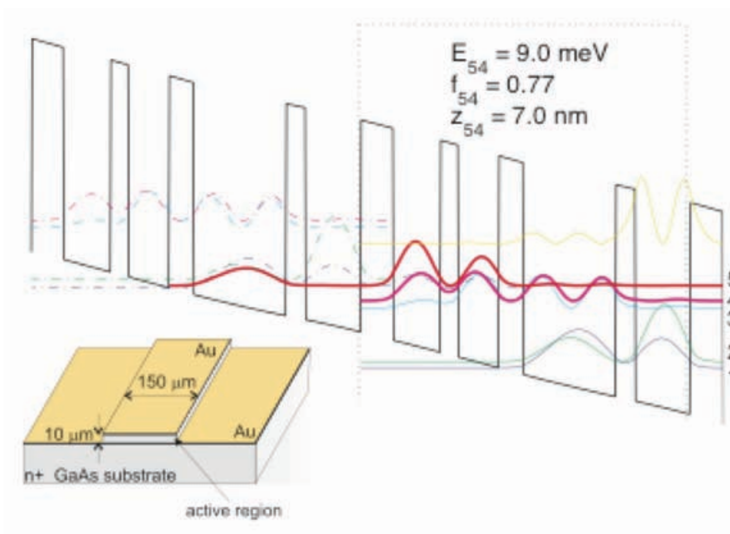

Figure 12 - Conduction band electron energy level diagram in a typical QCL structure.

many commercial molecular gas lasers operating in the THz, but in a far more compact, reliable, and maintenance-free semiconductor device rather than an optical table-sized tube laser. Many of the THz lasers designed at Sandia (see following table) were grown before the some of the growth refinements were resolved and hence the reason some did not work is not yet clear between design, growth or processing. The latter was clearly identified in many of the cases and as discussed in the processing section only came close to being resolved at the projects end. The last two are designed for removal of the substrate to create a metal-metal waveguide and the development of this process is still under development, thus the lasers are untested.

Sample Number	Design Frequency (μm)	Laser Operation?
EA 0846	73	No
EA 0873	70	No – regrown as 931
EA 0931	104	Yes
EA 0936	69	No- model code error
EA 0937	103	No- 5.1% growth error
EA 0938	73	No- model code error
EA 0991	91	No – test structure 6.7% growth error bad processing
EA 0992	78	No- 3% growth error
EA 1125	140	In process development
EA 1131	1100	In process development

EA 0931 (a regrowth of 873) was the first THz QC fabricated at Sandia that we were able to measure light output. The L-I-V is shown in fig. Figure 13 .

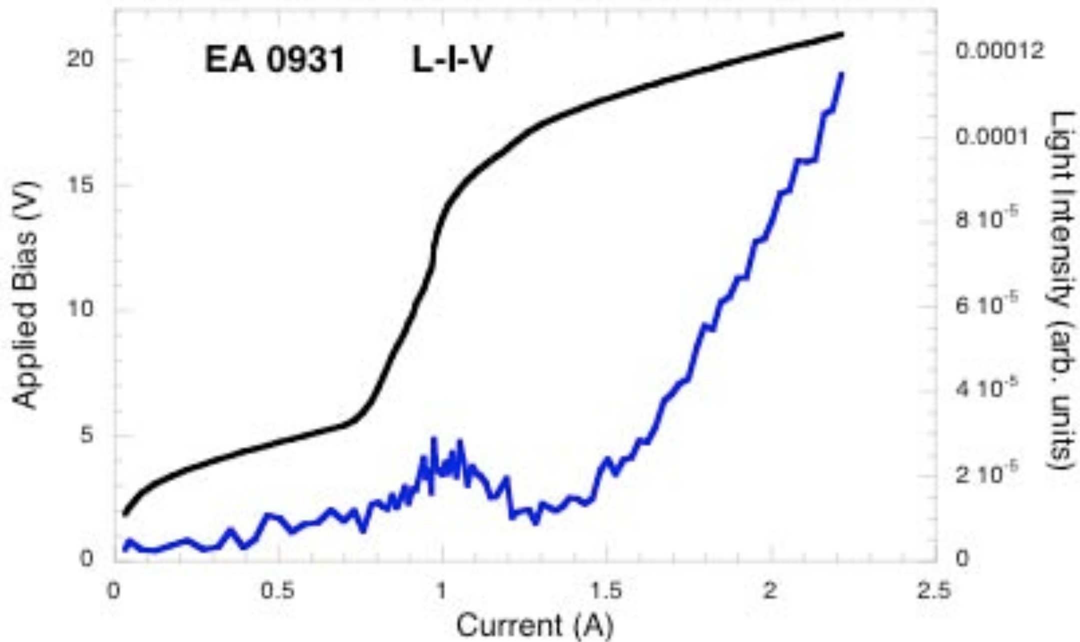

Figure 13 - First Sanda THz QC L-I-V

Appendix I: List of refereed publications and presentations

Publications

1. B. S. Williams and H. Callebaut and S. Kumar and Q. Hu and J. L. Reno, "3.4-THz quantum cascade laser based on longitudinal-optical-phonon scattering for depopulation", *Appl. Phys. Lett*., **82**, 1015 (2003)

2. B. S. Williams and S. Kumar and H. Callebaut and Q. Hu and J. L. Reno, “3.4 THz quantum cascade laser operating above liquid nitrogen temperature”, *Elec. Lett*., **39**, 915 (2003)

3. H. Callebaut and S. Kumar and B. S. Williams and Q. Hu and J. L. Reno, "Analysis of transport properties of tetrahertz quantum cascade lasers", *Appl. Phys. Lett*., **83**, 207 (2003)

4. B. S. Williams and S. Kumar and H. Callebaut and Q. Hu and J. L. Reno, "Terahertz quantum-cascade laser at lambda approximately=100 μm using metal waveguide for mode confinement", *Appl. Phys. Lett*., **83**, 2124 (2003)

5. B. S. Williams and S. Kumar and H. Callebaut and Q. Hu and J. L. Reno, "Terahertz quantum-cascade laser operating up to 137 K", *Appl. Phys. Lett*., **83**, 5142 (2003)

6. H. Callebaut and S. Kumar and B. S. Williams and Q. Hu and J. L. Reno, "Importance of electron-impurity scattering for electron transport in terahertz quantum-cascade lasers", *Appl. Phys. Lett*., **84**, 645 (2004)

7. Q. Hu and B. S. Williams and S. Kumar and H. Callebaut and J. L. Reno, “Terahertz quantum cascade lasers based on resonant phonon scattering for depopulation”, *Phil. Trans. Royal Soc. London, Ser. A*, **362**, 233 (2004)

8. S. Kumar and B. S. Williams and S. Kohen and Q. Hu and J. L. Reno, “Continuous-wave operation of terahertz quantum-cascade lasers above liquid-nitrogen temperature”, *Appl. Phys. Lett*., **84**, 2494 (2004)

9. B. S. Williams and S. Kumar and Q. Hu and J. L. Reno, “Resonant-phonon terahertz quantum-cascade laser operating at 2.1 THz (lambda [asymptotically equal to] 141 μm”, *Elec. Lett*., **40**, 431 (2004)

10. B. S. Williams and S. Kumar and H. Callebaut and S. Kohen and Qing Hu and J. L. Reno, “Terahertz quantum cascade lasers using resonant-phonon depopulation and metal-metal waveguides”, ”, *Proc. SPIE,* **5365**, 194 (2004)

Invited Presentations

1. "Quantum Cascade Lasers", LANL, October 2001.
2. "Quantum Cascade Lasers", University of Illinois, Champagne-Urbana, March 2004.
3. "Solid-State THz Developments", Laserion Workshop, June, 2004.
4. "Quantum Cascade Lasers and THz Detectors", PNNL, August, 2004.

Appendix II: Wet Etches

Wet Etches

During processing of the THz lasers, contact must be made from the base of an etched waveguide to he top of the etched waveguide, a height difference typically between 4 and 10 µm. To ensure contact during this metal deposition step, the sidewall of the waveguide or mesa must not be reentrant. From October 2003 through March 2004, a variety of wet etches were performed in order to develop a process that resulted in sloped or curved, non-reentrant sidewalls for orthogonal crystallographic orientations. A few of the etches had useable sidewalls in orthogonal crystal planes; however, the etches were unusable due to pitting caused by bubble formation during the etch. Typically, the etches studied yielded sloped sidewalls along one crystal plane but reentrant sidewalls on the orthogonal crystal plane. Laser waveguides can be fabricated using these etches provided that the waveguide is properly oriented to the correct crystal plane. However, round mesas (e.g. LEDs) or mesas that require contact from orthogonal directions (e.g. detectors) require that the sidewalls be non-reentrant in orthogonal crystallographic orientations.

Phosphoric acid

The phosphoric acid series is very good for etching laser waveguides, as long as the waveguide is properly aligned to the correct crystal plane. Typically, one planar direction has a sloped sidewall at an angle of about 55º while the orthogonal sidewall is reentrant. A small vertical drop is sometimes observed in the sloped sidewall, typically due to aging effects of the acid solution.

H_3PO_4:H_2O_2:H_2O (1:1:1), aged 0 min: etch rate = 6.6 µm/min

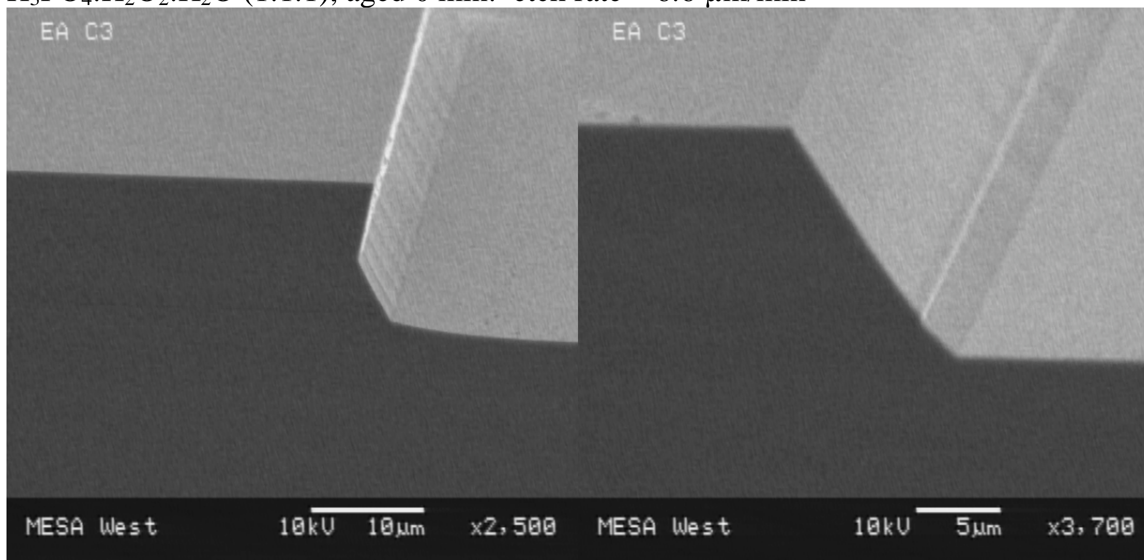

EA1032 with 0 min old H_3PO_4:H_2O_2:H_2O (1:1:1).

H_3PO_4:H_2O_2:H_2O (1:1:1), aged 30 min: etch rate = 6.4 µm/min

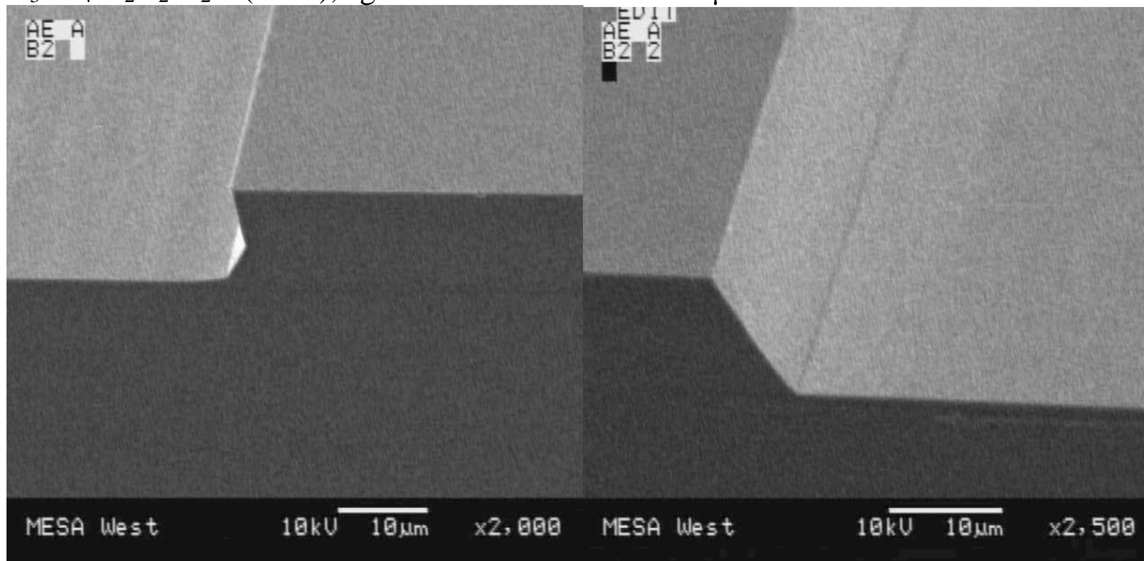

EA1032 etched with H_3PO_4:H_2O_2:H_2O (1:1:1), aged 30 min.

H_3PO_4:H_2O_2:H_2O (1:1:1), aged 60 min: etch rate = 5.6 µm/min

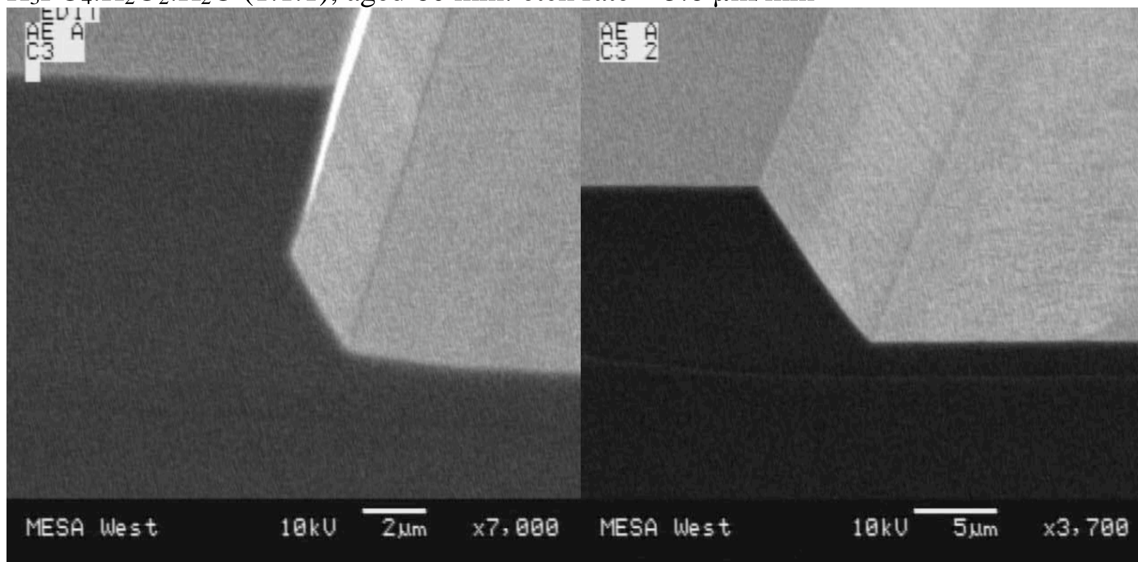

EA1032 etched with H_3PO_4:H_2O_2:H_2O (1:1:1), aged 60 min.

H_3PO_4:H_2O_2:H_2O (2:1:2), aged 0 min: etch rate = 6.9 µm/min

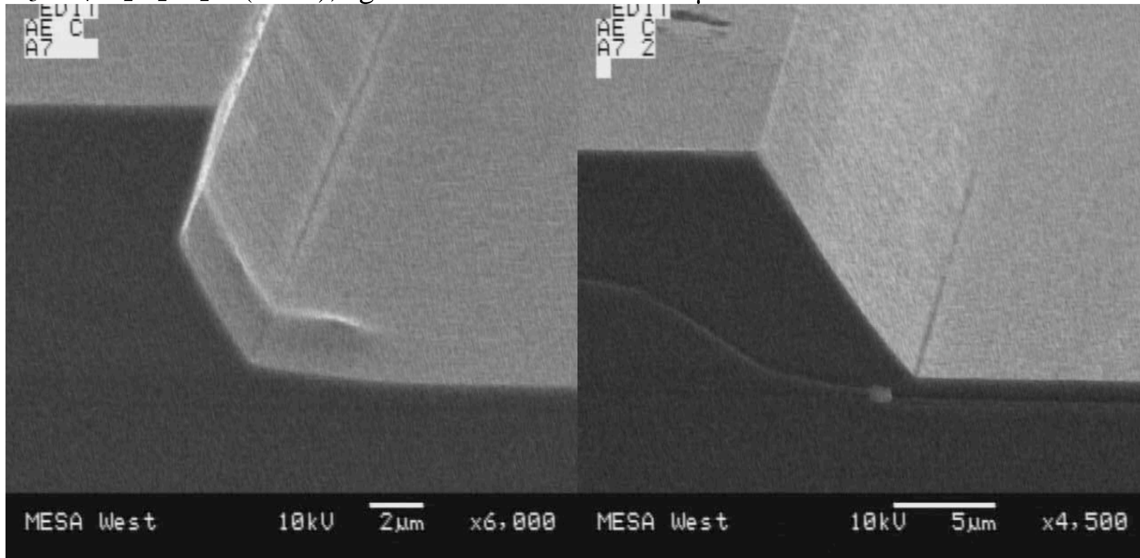

EA1032 etched with 0 min old H_3PO_4:H_2O_2:H_2O (2:1:2)

H_3PO_4:H_2O_2:H_2O (2:1:2), aged 30 min: etch rate = 4.0 µm/min

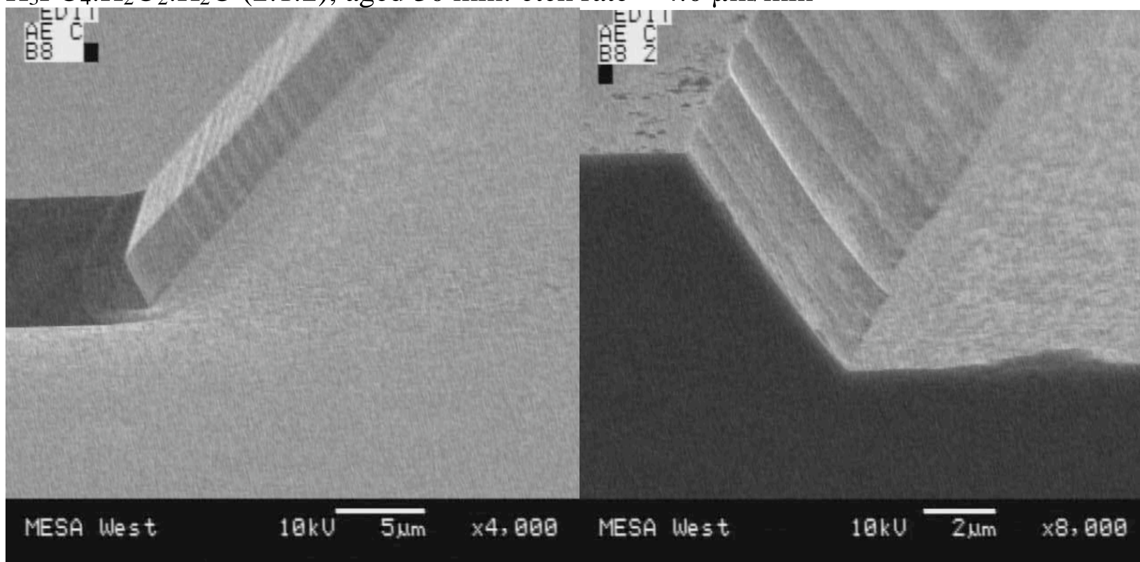

EA1032 etched with 30 min old H_3PO_4:H_2O_2:H_2O (2:1:2).

H_3PO_4:H_2O_2:H_2O (2:1:2), aged 60 min: etch rate = 3.7 µm/min

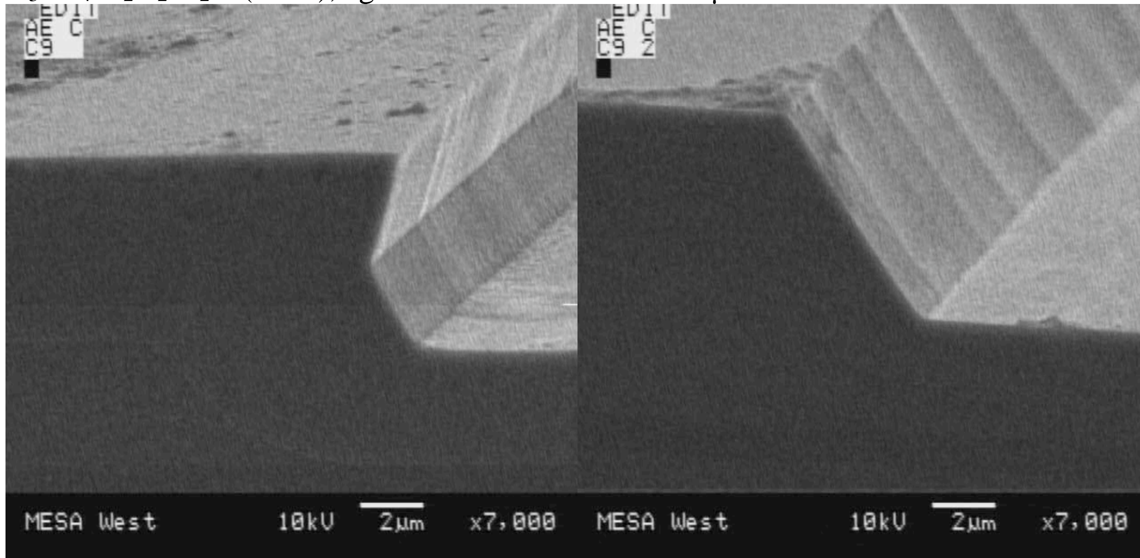

EA1032 etched with 60 min old H_3PO_4:H_2O_2:H_2O (2:1:2).

H_3PO_4:H_2O_2:H_2O (1:1:5), aged 0 min: etch rate = 1.7 µm/min

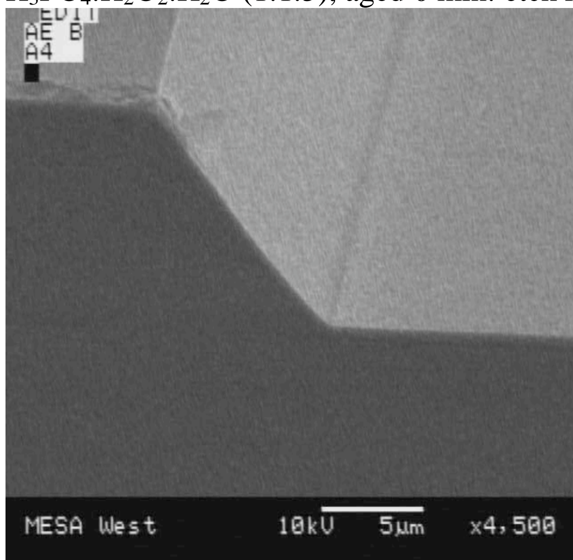

EA1032 etched with 0 min old H_3PO_4:H_2O_2:H_2O (1:1:5).

H_3PO_4:H_2O_2:H_2O (1:1:5), aged 30 min: etch rate = 0.87 μm/min

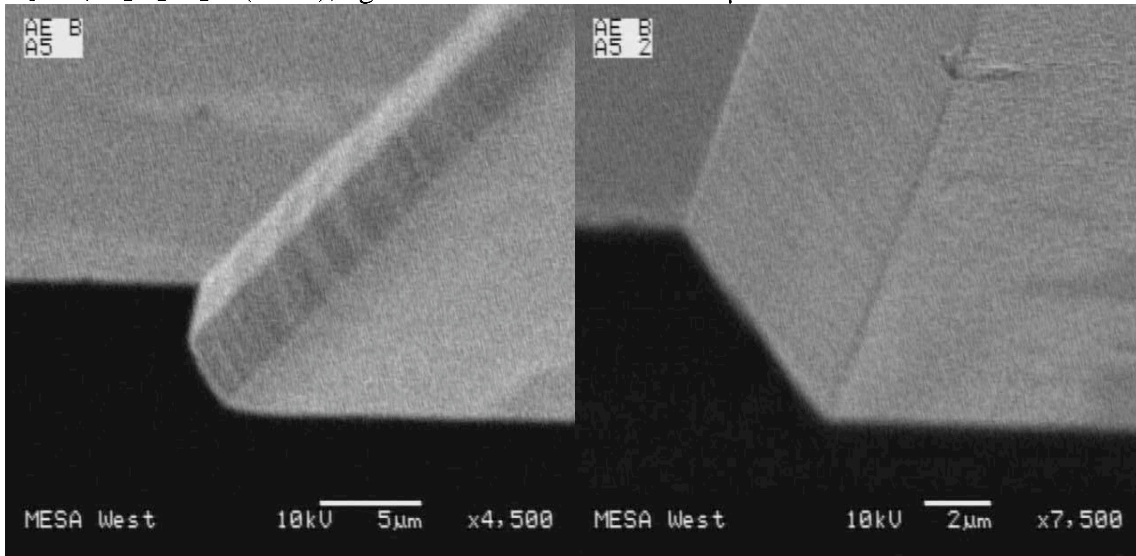

EA1032 etched with 30 min old H_3PO_4:H_2O_2:H_2O (1:1:5).

H_3PO_4:H_2O_2:H_2O (1:1:5), aged 60 min: etch rate = 1.4 μm/min

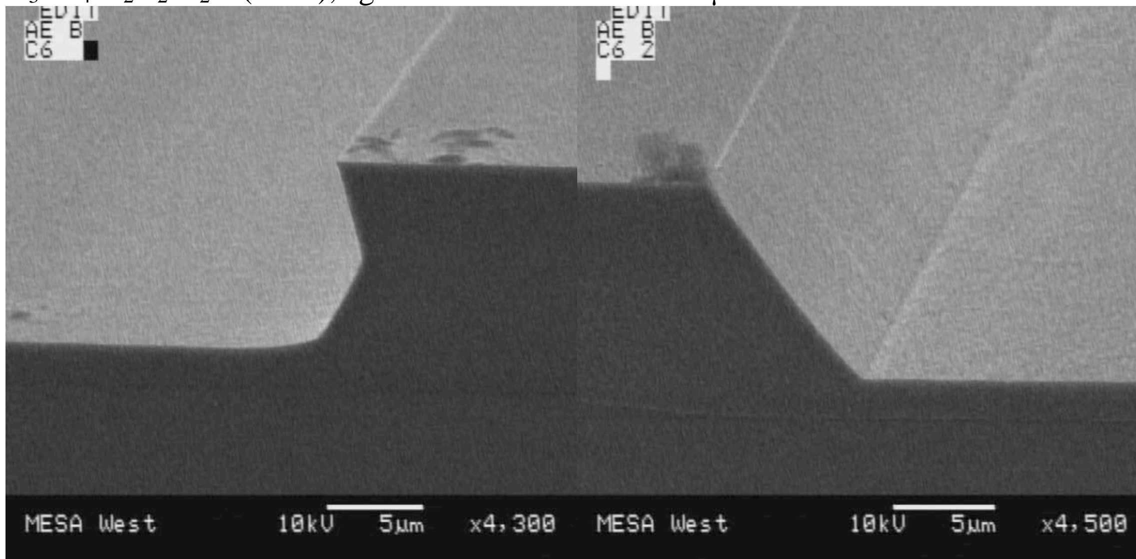

EA1032 etched with 60 min old H_3PO_4:H_2O_2:H_2O (1:1:5).

H_3PO_4:H_2O_2:H_2O (1:4:45): etch rate = 0.39 μm/min

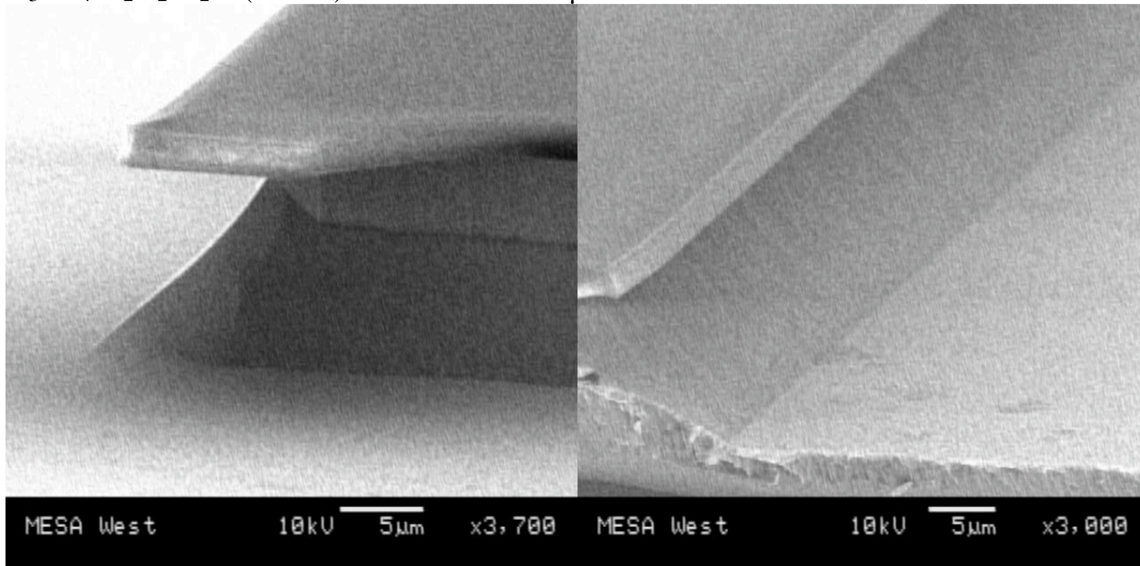

GaAs etched with H_3PO_4:H_2O_2:H_2O (1:4:45).

H_3PO_4:H_2O_2:H_2O (1:1:10): etch rate = 0.45 μm/min

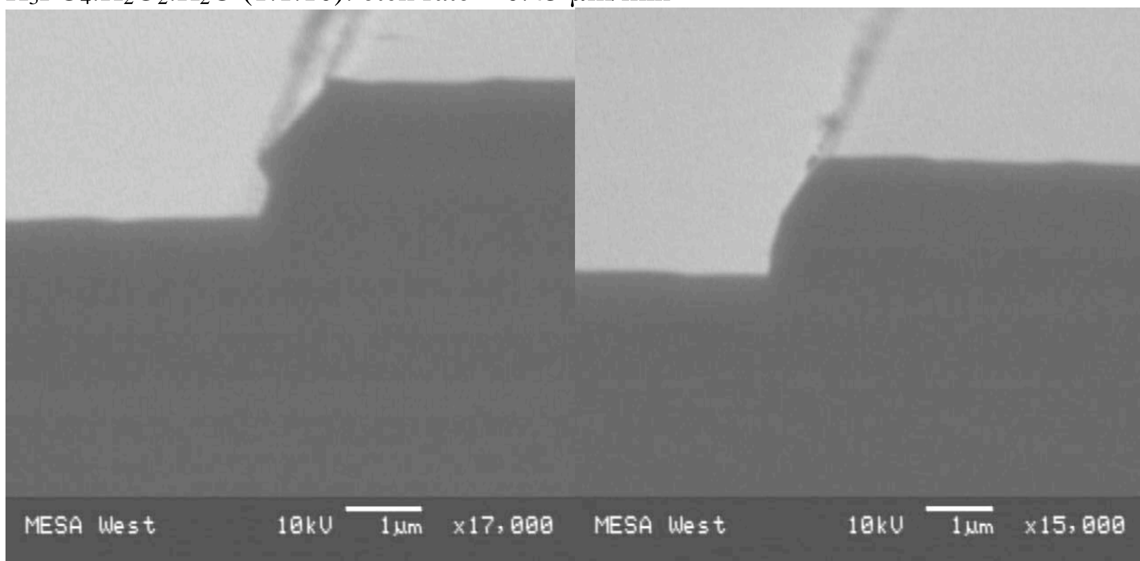

EB2013 (InP based) etched with H_3PO_4:H_2O_2:H_2O (1:1:10).

Hydrofluoric acid

The fluorine based etches give a very different profile than the phosphorous based etches. The sidewalls have a concave curve to them. At times a small undercut layer is observed. The greater problem is the lateral etch rate is approximately three times faster than the vertical etch rate, resulting in a huge undercut. Thus, this etch family is not useful for typical waveguide widths and depths.

$HF:H_2O_2:H_2O$ (1:4:4): etch rate = 7.4 µm/min

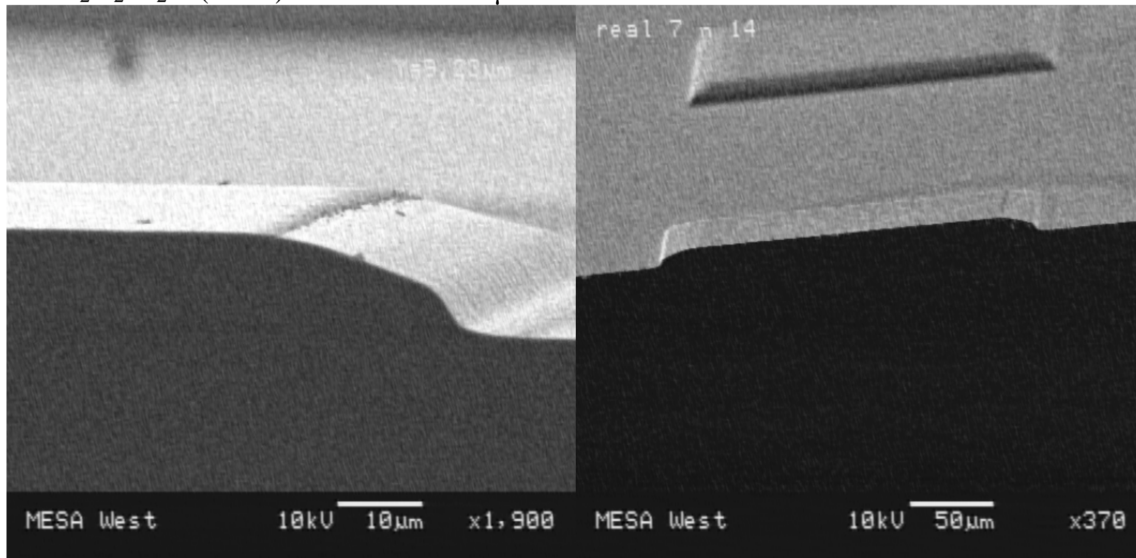

EA1032 etched with $HF:H_2O_2:H_2O$ (1:4:4).

$HF:H_2O_2:H_2O$ (1:4:20): etch rate = 1.2 µm/min

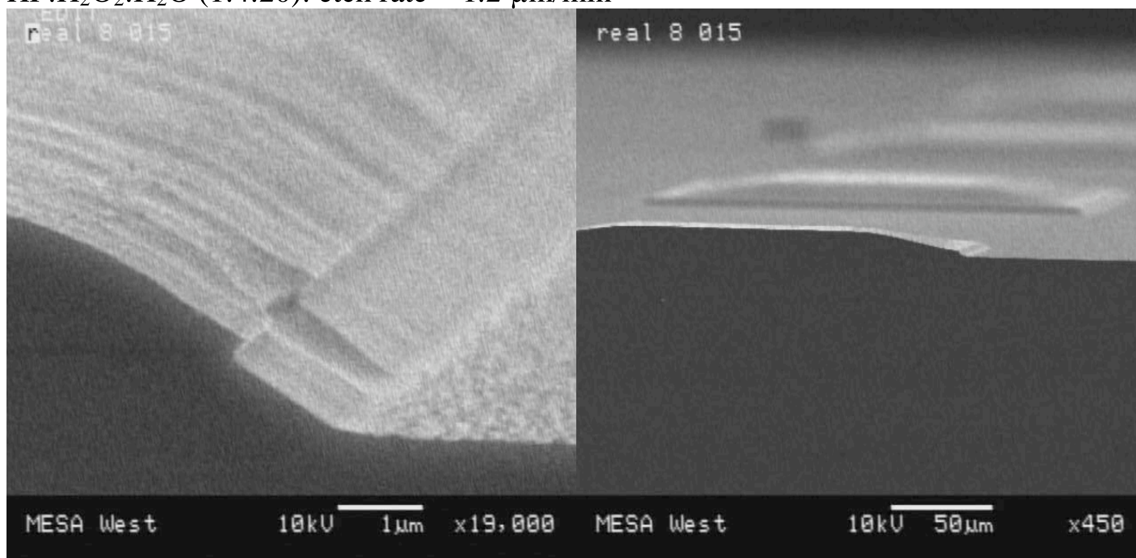

EA1032 etched with $HF:H_2O_2:H_2O$ (1:4:20).

$HF:HNO_3:H_2O$ (1:1:1): etch rate ~ 5 um/min.

$HF:HNO_3:H_2O$ (1:1:10): no etching observed.

Ammonium hydroxide

The etch results for ammonium hydroxide are similar to those from the phosphoric acid family in that a sloped sidewall is observed in one direction and a reentrant sidewall is observed in the orthogonal direction. The shape of the reentrant sidewall differs between the two types of etches but the conclusion is the same: an etch useful for making waveguides only when proper alignment to the correct crystal plane is made.

NH_4OH: $H_2O_2:H_2O$ (3:1:14): etch rate = 1.4 μm/min

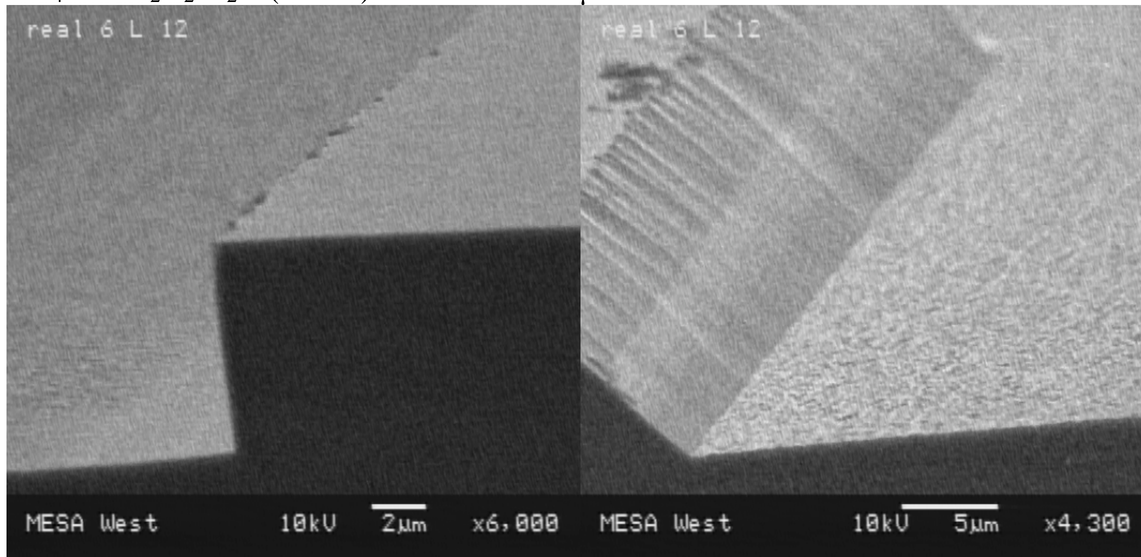

EA1032 etched with NH_4OH: $H_2O_2:H_2O$ (3:1:14).

Hydrobromic acid

The bromine based etches were practically isotropic, except for a slight overhang at the top of the mesa. Though small, this overhang is large enough to create a shadow and prevent the deposited metal from making continuous contact from the bottom of the mesa to the top of the mesa. Occasional trenching and pitting was also observed.

$HBr:HNO_3:H_2O$ (1:1:10), aged 2 hours:

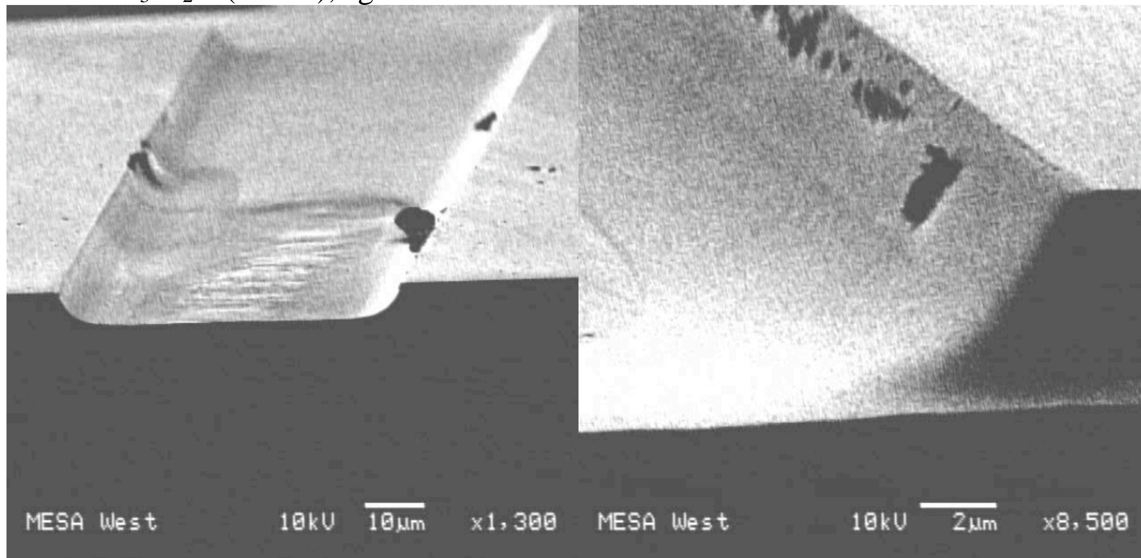

EB2024 (InP based) etched with 2 hour old $HBr:HNO_3:H_2O$ (1:1:10).

$HBr:HNO_3:H_2O$ (1:1:10), aged 3.5 days:

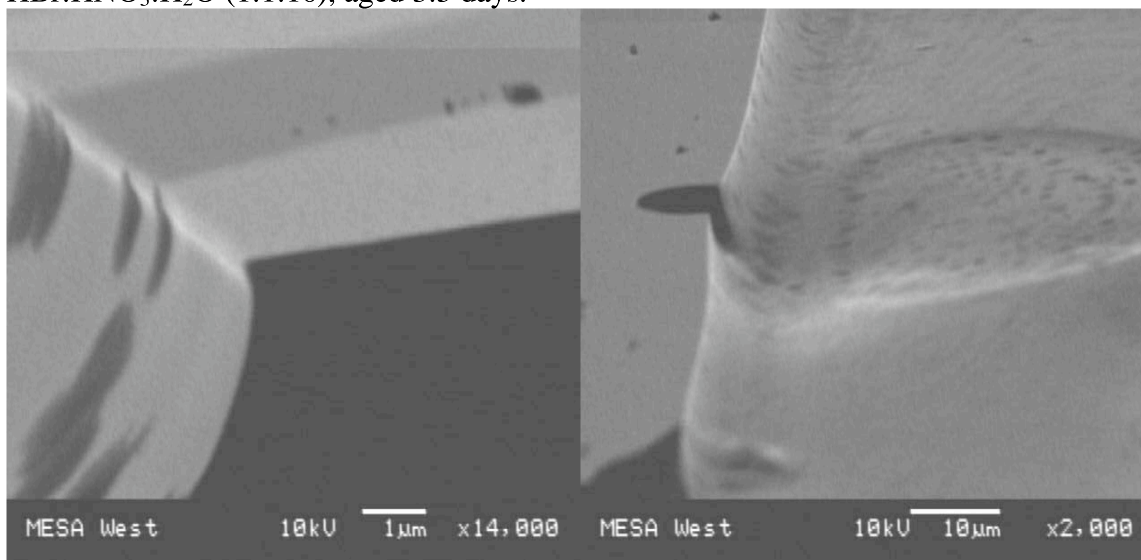

EA 931 etched with 3.5 day old $HBr:HNO_3:H_2O$ (1:1:10).

$HBr:HNO_3:H_2O$ (1:1:10), aged 8 days:

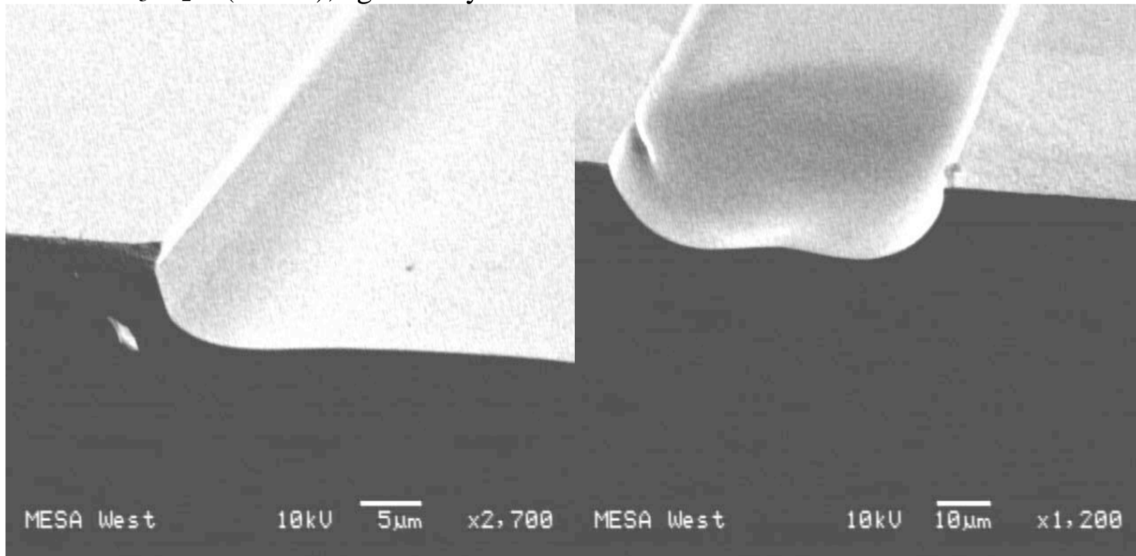

EA 995 etched with 8 day old $HBr:HNO_3:H_2O$ (1:1:10).

$HBr:HNO_3:H_2O$ (1:1:10), aged 12.5 days:

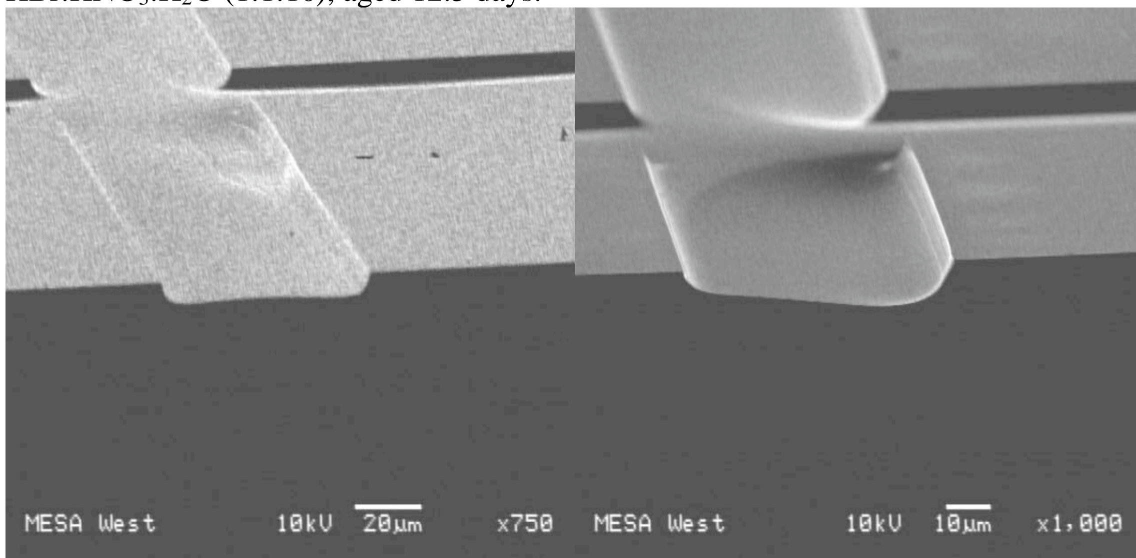

EB2024 (InP based) etched with 12.5 day old $HBr:HNO_3:H_2O$ (1:1:10).

Hydrochloric acid

The chlorine based etches resulted in isotropicly etched sidewalls in orthogonal directions. However, bubbles form on the sample surface during the etch, resulting in non-uniform etching. The etch rate under the bubble is much higher than in surrounding areas. Trenching was also observed near the mask edge.

HCl: H_2O_2:H_2O (40:4:1): etch rate = 0.31 μm/min

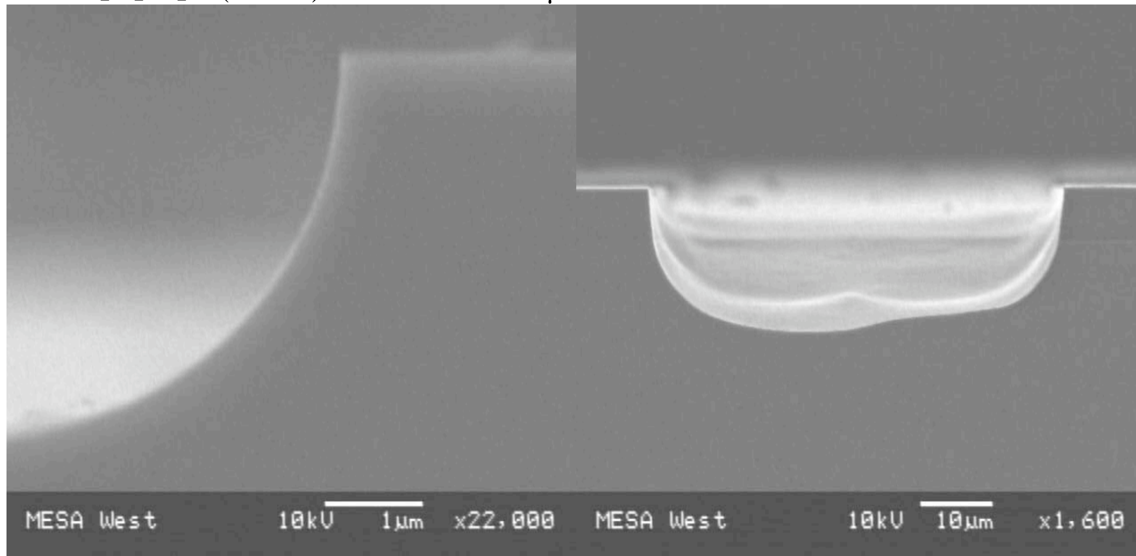

EA993 etched with HCl: H_2O_2:H_2O (40:4:1).

HCl: H_2O_2:H_2O (60:4:1):

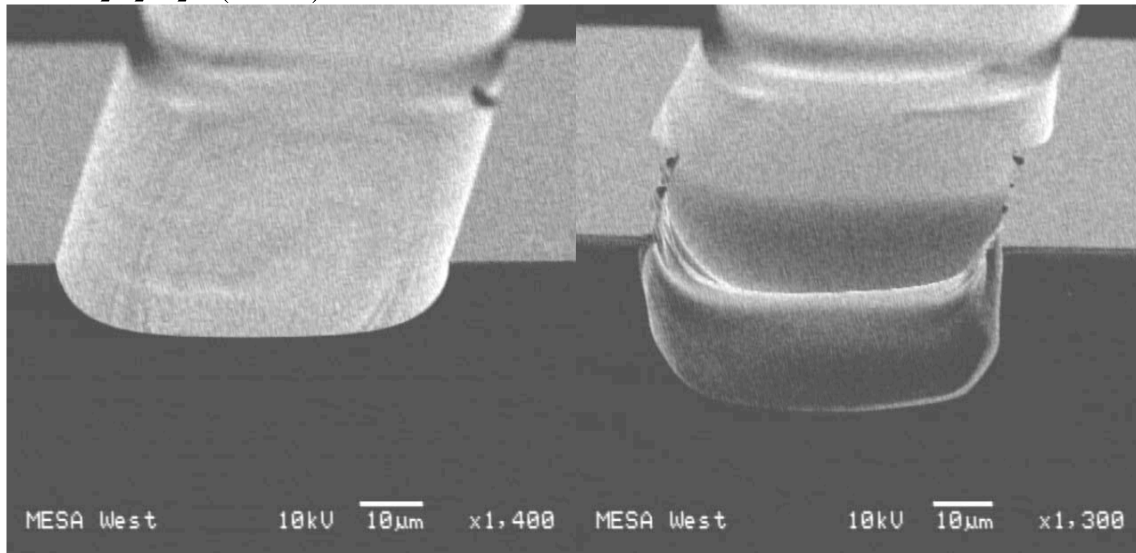

EA 995 etched with HCl: H_2O_2:H_2O (60:4:1).

Appendix III: Insulator Tests

Insulator tests versus anneal temperature:

Insulator 1: SiNx
Problems: SiNx forms many small bubbles, which seldom rupture, when RTA'd at high temperatures

Insulator 2: SiO2
Problems: SiO2 partially delaminates and forms large bubbles, some of which rupture, when coated with TiAu and RTA'd, even at lower temperatures (360 C).

Insulator 3: SiNx/SiO2
Each dielectric (SiO2, SiNx) absorbs at slightly different wavelengths, so processing capabilities are needed for both. Using a thin layer of SiNx underneath a thick layer of SiO2 appears to relieve some of the stress from the SiO2.

Insulator 4: SiO2 (High temperature deposition – 350 C)
Appears to remove bubbling problems observed in the lower temperature SiO2 films.

First three insulators as a function of RTA temperature.

RTA: 460 °C

	SiO2	SiN	SiN/SiO2
No Metal	Smooth	Many small bubbles	Many small bubbles
Metal	Large bubbles, some bubbles ruptured	Many small bubbles	Many small bubbles

RTA: 420 °C

	SiO2	SiN	SiN/SiO2
No Metal	Smooth	Smooth	Smooth
Metal	Large bubbles, some bubbles ruptured	Smooth	Smooth

RTA: 360 °C

	SiO2	SiN	SiN/SiO2
No Metal	Smooth	Smooth	Smooth
Metal	Large bubbles, some bubbles ruptured	Smooth	Smooth

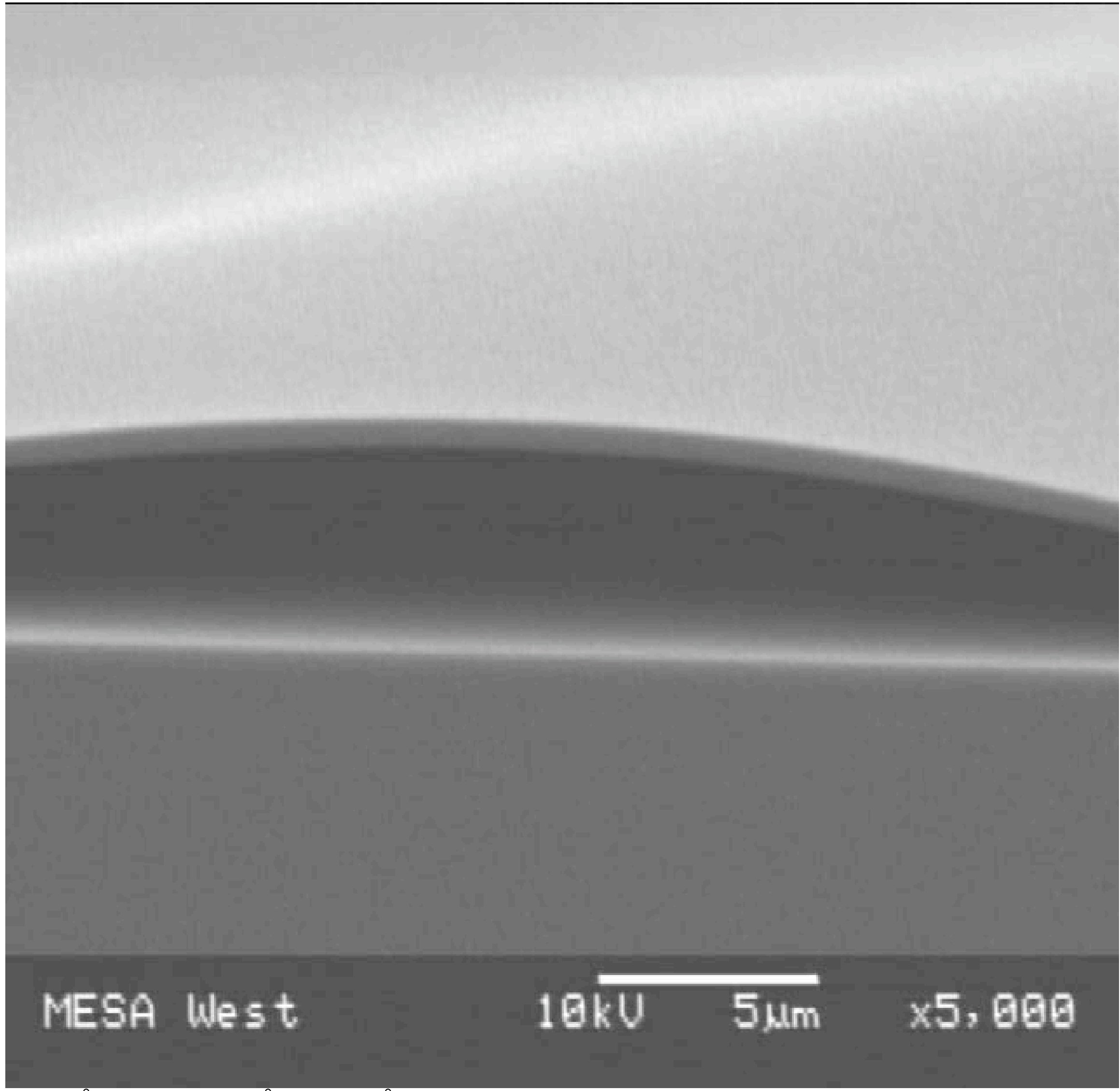

4000 Å SiO_2 w/ 200Å Ti/ 300Å Au, RTA: 460 °C, 15s, 20s ramp.
SEM close-up of bubble formed beneath SiO2 that did not break off.

Insulator tests versus material

METAL ONLY

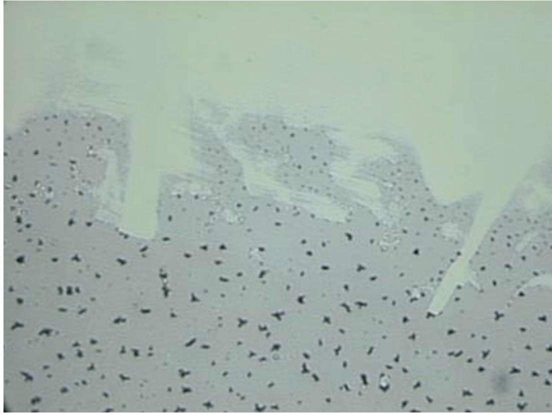

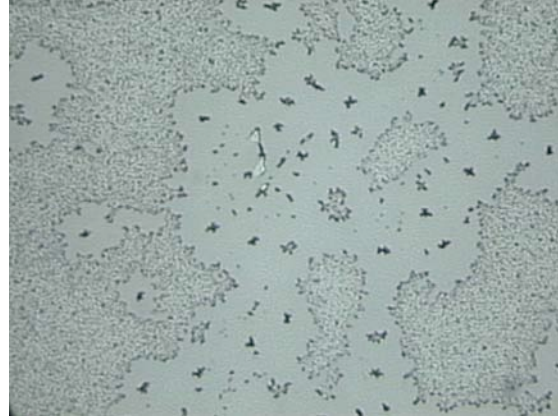

Piece 2: Blank GaAs covered with 200 Ti/ 500 Au, after RTA (460 °C, 15s).

Piece 1: Blank GaAs covered with 200 Ti/ 300 Au, after RTA (460 °C, 15s).

Though both piece 1 and piece 2 are just blank GaAs, the metal has changed significantly on piece 2, exhibiting three different phases, while the metal remains fine on piece 1. Perhaps this is due to the location of the pieces in the RTA.

Oxide on GaAs

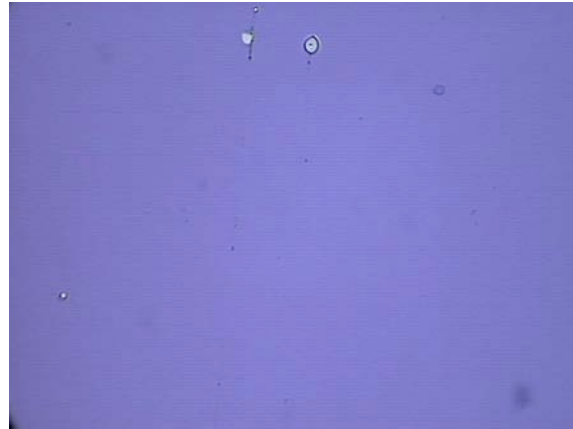

Piece 12: Blank GaAs with 4000 Å SiO_2, after RTA (460 °C, 15 s).

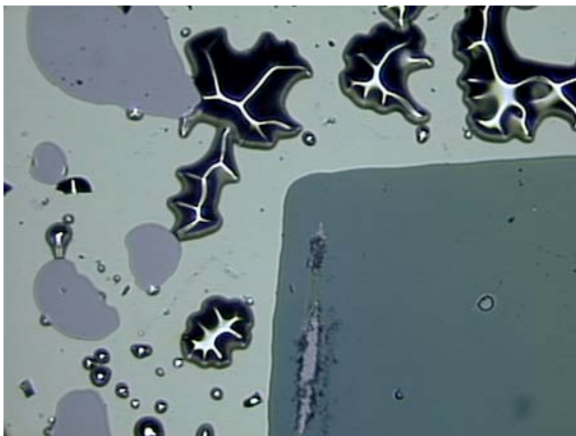

Piece 5: Blank GaAs with 4000 Å SiO_2 and 200 Ti/ 300 Au, after RTA (460 °C, 15 s).

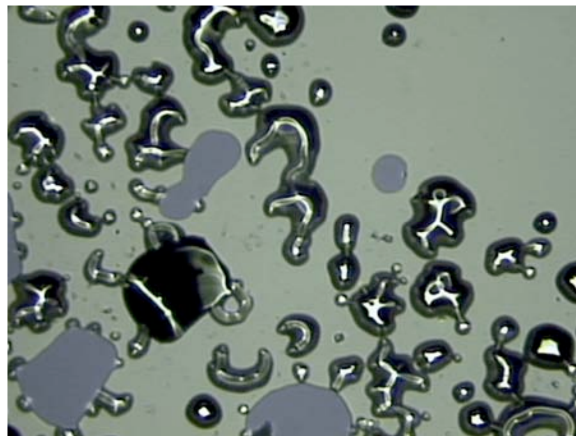

Piece 6: Blank GaAs with 4000 ÅSiO_2 and 200 Ti/ 500 Au, after RTA (460 °C, 15 s).

No bubbling of the oxide to speak of when there is just oxide on GaAs. However, with the metal added, the SiO_2 bubbles and sometimes pops off. This is evident by comparing the green color of the oxide with the grey color of the popped bubbles. The amount of bubbles did vary from piece to piece, and even across each piece. Piece 5 was almost entirely covered with bubbles, while piece 6 had bubbles predominantly on one side.

Nitride on GaAs

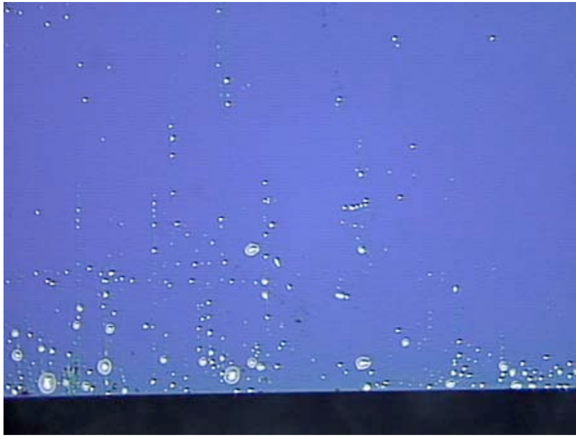

Piece 11: Blank GaAs with 4000 Å SiNx, after RTA (460 °C, 15 s).

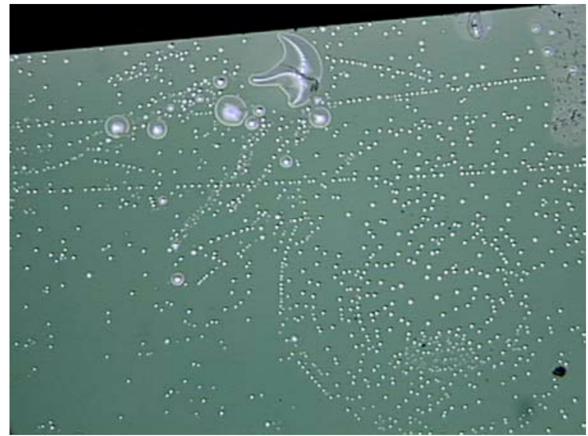

Piece 9: EA 1032 with 4000 Å SiNx, after RTA (460 °C, 15 s).

Piece 5: Blank GaAs with 4000 Å SiNx and 200 Ti/ 300 Au, after RTA (460 °C, 15 s).

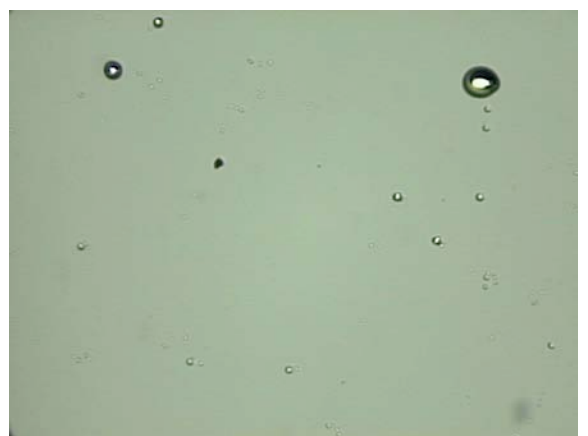

Piece 6: Blank GaAs with 4000 Å SiNx and 200 Ti/ 500 Au, after RTA (460 °C, 15 s).

Bubbles formed in the nitride without any metal. The addition of metal does not appear to make the bubbles any worse. However, the amount of bubbles did vary from piece to piece, as well as across each piece.

Si substrate

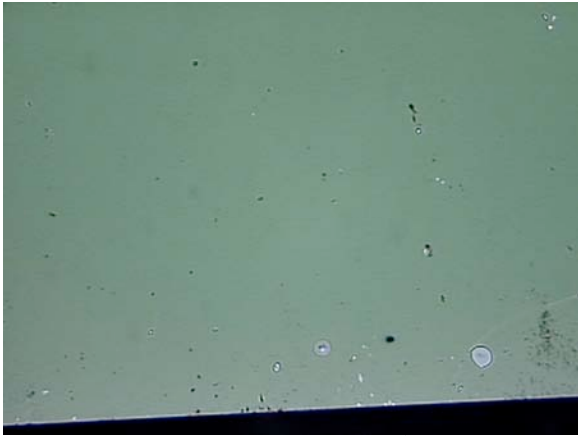

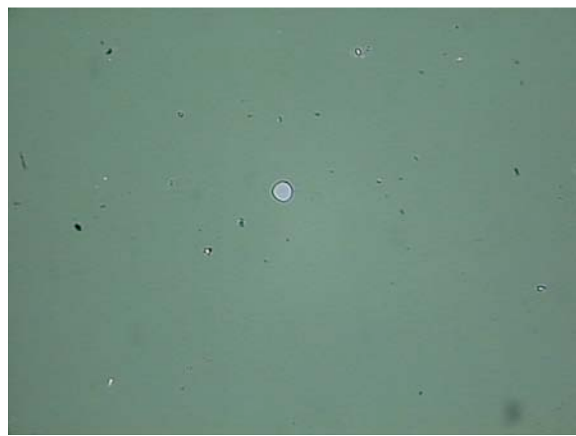

Piece 13: Blank Si with 4000 Å SiNx, after RTA (460 °C, 15 s).

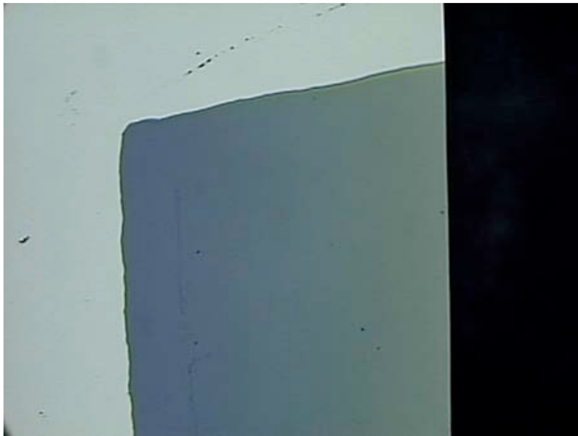

Piece 14: Blank Si with 4000 Å SiO_2 and 200 Ti/ 300 Au, after RTA (460 °C, 15 s).

No bubbles to speak of in either the nitride or the oxide on Si substrate.

Summary

In conclusion, the nitride (4000 Å) bubbled on the GaAs substrates both with and without metal on top of the nitride. The oxide (4000 Å) bubbled on the GaAs substrates only with the addition of the metal layer. For both the oxide and nitride, the bubbling was a result of the oxide/nitride separating from the substrate. The amount of bubbling differed from piece to piece and across each piece.

Neither the oxide nor the nitride bubbled on the Si substrate.

The metal changed phases on one piece where it was deposited directly onto the GaAs substrate, but did not change on the other piece.

The variations in the location and amount of bubbles as well as the difference in the metals on the two bare GaAs pieces suggests that the location of the pieces in the RTA plays a significant role in the success of the process. Perhaps there is a "hotspot" in the RTA that is at a much higher temperature than desired which is causing the bubbling/metal failure.

Distribution

1	MS 0601	John Reno, 01123
1	MS 0601	Larry Stephenson, 01123
1	MS 0601	Dan Barton, 01123
1	MS 0603	Sally Samora, 01743
1	MS 0603	Chuck Fuller, 01743
1	MS 0603	Erik Young, 01743
1	MS 0603	Mike Mangan, 01743
1	MS 0603	Mike Wanke, 01743
1	MS 0603	Jim Hudgens, 01743
1	MS 1071	Jay Jakubczak, 01703
1	MS 1077	Tom Zipperian, 01720
1	MS 1078	Stephen Martin, 01707
1	MS 1079	Marion Scott, 01700
1	MS 1421	Jerry Simmons, 01120
1	MS 1423	Robert Foltynowicz, 01128
1	MS 1427	Julia Phillips, 01100
1	MS 9018	Central Technical Files, 08945-1
2	MS 0899	Technical Library, 09616
1	MS 0161	Patent and Licensing Office, 01150
1	MS 0123	Donna Chavez, LDRD Office, 01011